Acta Pharmaceutica Sinica B 2024;14(12):5286–5304

Chinese Pharmaceutical Association
Institute of Materia Medica, Chinese Academy of Medical Sciences

Acta Pharmaceutica Sinica B

www.elsevier.com/locate/apsb
www.sciencedirect.com

ORIGINAL ARTICLE

Targeted inhibition of Gus-expressing *Enterococcus faecalis* to promote intestinal stem cell and epithelial renovation contributes to the relief of irinotecan chemotoxicity by dehydrodiisoeugenol

Ruiyang Gao[a,†], Bei Yue[a,†], Cheng Lv[b], Xiaolong Geng[a], Zhilun Yu[a], Hao Wang[a], Beibei Zhang[a], Fangbin Ai[a], Ziyi Wang[a], Donghui Liu[a], Zhengtao Wang[a,*], Kaixian Chen[a,c,*], Wei Dou[a,*]

[a]*The MOE Key Laboratory of Standardization of Chinese Medicines, Shanghai Key Laboratory of Compound Chinese Medicines, and the SATCM Key Laboratory of New Resources and Quality Evaluation of Chinese Medicines, Institute of Chinese Materia Medica, Shanghai University of Traditional Chinese Medicine, Shanghai 201203, China*
[b]*Centre for Chinese Herbal Medicine Drug Development Limited, Hong Kong Baptist University, Hong Kong SAR 999077, China*
[c]*Shanghai Institute of Materia Medica, Chinese Academy of Sciences, Shanghai 201210, China*

Received 26 March 2024; received in revised form 25 June 2024; accepted 26 July 2024

KEY WORDS

Irinotecan;
Intestinal mucositis;
β-Glucuronidase;
Enterococcus faecalis;
Intestinal stem cells;
Epithelial regeneration;

Abstract Irinotecan (CPT11) chemotherapy-induced diarrhea affects a substantial cancer population due to *β*-glucuronidase (Gus) converting 10-*O*-glucuronyl-7-ethyl-10-hydroxycamptothecin (SN38G) to toxic 7-ethyl-10-hydroxycamptothecin (SN38). Existing interventions primarily address inflammation and Gus enzyme inhibition, neglecting epithelial repair and Gus-expressing bacteria. Herein, we discovered that dehydrodiisoeugenol (DDIE), isolated from nutmeg, alleviates CPT11-induced intestinal mucositis alongside a synergistic antitumor effect with CPT11 by improving weight loss, colon shortening, epithelial barrier dysfunction, goblet cells and intestinal stem cells (ISCs) loss, and wound-healing.

*Corresponding authors.
E-mail addresses: ztwang@shutcm.edu.cn (Zhengtao Wang), kxchen@simm.ac.cn (Kaixian Chen), douwei@shutcm.edu.cn (Wei Dou).
[†]These authors made equal contributions to the work.
Peer review under the responsibility of Chinese Pharmaceutical Association and Institute of Materia Medica, Chinese Academy of Medical Sciences.

https://doi.org/10.1016/j.apsb.2024.09.018

Gus bacteria−host−irinotecan axis; Dehydrodiisoeugenol

The anti-mucositis effect of DDIE is gut microbiota-dependent. Analysis of microbiome profiling data from clinical patients and CPT11-induced mucositis mice reveals a strong correlation between CPT11 chemotoxicity and Gus-expressing bacteria, particularly *Enterococcus faecalis* (*E. faecalis*). DDIE counters CPT11-induced augmentation of *E. faecalis*, leading to decreased intestinal Gus and SN38 levels. The Partial Least Squares Path Model (PLS-PM) algorithm initially links *E. faecalis* to dysregulated epithelial renovation. This is further validated in a 3D intestinal organoid model, in which both SN38 and *E. faecalis* hinder the formation and differentiation of organoids. Interestingly, colonization of *E. faecalis* exacerbates CPT11-induced mucositis and disturbs epithelial differentiation. Our study unveils a microbiota-driven, epithelial reconstruction-mediated action of DDIE against mucositis, proposing the 'Gus bacteria−host−irinotecan axis' as a promising target for mitigating CPT11 chemotoxicity.

1. Introduction

Irinotecan (CPT11), a semi-synthetic analog of the natural alkaloid camptothecin, is a widely utilized anticancer agent for various malignancies, including colorectal, gastric, pancreatic, ovarian, and other tumors[1,2]. However, the clinical application of CPT11 is hampered by the onset of delayed diarrhea and consequential damage to the intestinal mucosa[3]. The overall incidence of CPT11-induced diarrhea is substantial, reaching up to 87%, with grade 3−4 diarrhea occurring in 30%−40% of cases. Prolonged diarrhea poses serious complications, including severe dehydration, electrolyte imbalance, acid-base disturbances, shock, and potential mortality[4].

The intestinal epithelium, acting as a pivotal barrier between the host and the external environment, consists of enterocytes, goblet cells, and stem cells, which collectively contribute significantly to the maintenance of gut homeostasis[5,6]. In the context of CPT11 chemotherapy, patients frequently endure severe diarrheal episodes associated with considerable epithelial damage[2]. CPT11 not only disrupts epithelial integrity but also diminishes the regenerative capability of the intestine, particularly affecting goblet cells and intestinal stem cells (ISCs)[7,8]. Goblet cells, crucial for mucus production, and stem cells, vital for epithelial renewal, are particularly susceptible to the cytotoxic effects of CPT11, resulting in a compromised mucosal barrier and a diminished regenerative response[7]. This exacerbation of epithelial injury and stem cell depletion plays a pivotal role in the severity of chemotherapy-induced gastrointestinal (GI) toxicity, necessitating further exploration for effective mitigation strategies.

Extensive research has elucidated the mechanisms behind CPT11-induced diarrhea, highlighting the enterohepatic recirculation of 7-ethyl-10-hydroxycamptothecin (SN38) and the involvement of bacterial β-glucuronidase (Gus)[9,10]. As a prodrug, CPT11 is initially metabolized by carboxylesterases and transformed into SN38. SN38 is significantly more potent than CPT11, showing 100 to 1000-fold higher efficacy in cell killing[11]. SN38 is metabolized into the non-toxic SN38 glucuronide (SN38G) by uridine diphosphate-glucuronosyltransferase in both the liver and intestine, and then excreted into the GI tract. However, SN38 can be regenerated from SN38G in the intestinal tract due to the action of the bacterial Gus enzyme, leading to a high concentration of SN38 in the intestine and causing delayed diarrhea, which limits the application of CPT11[9].

Recognizing the crucial role of bacterial Gus in SN38 regeneration, the ongoing development of Gus inhibitors emerges as a potential strategy to alleviate CPT11-induced GI toxicity[12]. Various Gus inhibitors, including amoxapine, antibiotics (penicillin, neomycin, streptomycin, ciprofloxacin), herbal medicines (baicalin, luteolin, gentisin), and synthesized compounds, have shown promising effects in mitigating CPT11-induced GI toxicity[13,14]. Additionally, studies have shown that herbal prescriptions such as PHY906 and Xiao Chai Hu Tang can alleviate CPT11 chemotoxicity, and this effect is linked to the inhibitory impact of the natural active component, baicalein, on the activity of the Gus enzyme[15,16]. Nevertheless, existing interventions for CPT11 chemotoxicity primarily target inflammation and Gus enzyme inhibition while neglecting Gus-expressing bacteria and intestinal epithelial repair.

In the extant human microbiome database, approximately 43% of microbial species possess the genetic coding for Gus (or possible candidate structures), including *Enterobacteriaceae*, *Bacteroides* spp., *Lactobacillus* spp., *Staphylococcus* spp., *Clostridium* clusters XIVa and IV[17]. Different Gus enzymes from various microbes exhibit distinct hydrolytic activities, with higher enzymatic activities observed in *Bacteroides uniformis*, *Clostridium paraputrificum*, *Clostridium clostridioforme*, and *Enterococcus faecalis* within the human colon[18,19]. Moreover, a growing body of evidence suggests a robust connection between the gut microbiota and the host's response to chemotherapeutic drugs[20]. However, there are few reports directly studying the modulation of Gus-expressing microbial populations to intervene in CPT11 chemotoxicity.

The seed of nutmeg (*Myristica fragrans* Houtt.) has historically been used in traditional medicine to alleviate discomfort in the digestive tract, abdominal pain, and persistent diarrhea[21]. Dehydrodiisoeugenol (DDIE) (Fig. 1A), a lignan isolated from nutmeg, exhibits diverse activities, including anti-tumor, anti-oxidant, anti-inflammatory, and hepatoprotective effects[22,23]. DDIE has been reported to attenuate acetic acid-induced enteritis[24], suggesting its potential as a novel agent in combating chemotherapy-induced GI toxicity. Nevertheless, the role of gut microbiota in the action of DDIE remains uncertain.

Our prior research revealed the therapeutic potential of berberine in alleviating CPT11-induced gut mucositis by acting as a non-competitive inhibitor against bacterial Gus enzyme[25]. Herein, we aim to clarify the efficacy of DDIE in alleviating CPT11-induced gut mucositis and explore the underlying microbiota-driven epithelial repair mechanism. The contributive role of Gus-generating microbiota, *E. faecalis*, in the action of DDIE in CPT11-injected colorectal tumor-bearing mice is investigated for the first time. This research employs fecal 16S rRNA

sequencing data from CPT11 chemotherapeutic patients and mucositis mice, CPT11/SN38 quantification, intestinal organoid culture, single-bacterium colonization, and Partial Least Squares Path Model (PLS-PM) analysis to elucidate a gut microbiota-driven mechanism by which DDIE alleviates CPT11 chemotoxicity.

2. Material and methods

2.1. Materials

DDIE [$C_{20}H_{22}O_4$, Chemical Abstracts Service (CAS): 2680-81-1; molecular weight (MW): 326.39; purity ≥98%] was purchased from Weikeqi Biotech (Sichuan, China). CPT11 ($C_{33}H_{38}N_4O_6 \cdot HCl \cdot 3H_2O$, CAS: 136572-09-3; MW: 677.19), ampicillin ($C_{16}H_{19}N_3O_4S \cdot 3H_2O$, CAS: 7177-48-2, MW: 403.45), neomycin ($C_{23}H_{46}N_6O_{13} \cdot 3H_2SO_4$, CAS: 1405-10-3, MW: 908.87), vancomycin ($C_{66}H_{75}Cl_2N_9O_{24} \cdot HCl$, CAS: 1404-93-9, MW: 1485.72), metronidazole ($C_6H_9N_3O_3$, CAS: 443-48-1, MW: 171.15), and SN38 ($C_{22}H_{20}N_2O_5$, CAS: 86639-52-3, MW: 392.40) were obtained from Dalian Meilun Biotech Co., Ltd. (Dalian, China). Diethylpyrocarbonate-treated water, dimethyl sulfoxide, paraformaldehyde (PFA), and diaminobenzidine were obtained from Sigma−Aldrich (Shanghai, China). Roswell Park Memorial Institute-1640, 100 U/mL penicillin/streptomycin, and fetal bovine serum were obtained from Gibco BRL (Grand Island, NY, USA). The primary antibodies against inducible nitric oxide synthase (iNOS, #18985-1-AP) and cyclooxygenase-2 (COX-2, #12375-1-AP) were obtained from Proteintech Group (Chicago, IL, USA). KI67 (#9449) and β-actin (#4970) were obtained from Cell Signaling Technology (Danvers, MA, USA). Rabbit antibodies against Zonula occludens 1 (ZO-1, A0659), Occludin (A2601), krüppel-like transcription factor 4 (KLF4, A13673), and mucin2 (MUC2, A4747) were obtained from ABclonal Technology (Wuhan, China). The enhanced chemiluminescence detection kit was purchased from Millipore (Billerica, MA, USA). TRIzol was obtained from Thermo Fisher Scientific (MA, USA). SYBR Green Premix Pro Taq HS qPCR Kit (Rox Plus) and *Evo M-MLV* real-time premix for quantitative polymerase chain reaction were purchased from Takara Biotechnology (Hunan, China).

2.2. Cell culture

NCM460 human normal intestinal epithelial cells and CT26 murine colon carcinoma cells were purchased from the American Type Culture Collection (Manassas, VA, USA) and cultured in Roswell Park Memorial Institute-1640 culture medium supplemented with 10% fetal bovine serum (Gibco BRL, Grand Island, NY, USA) in an incubator at 37 °C with 5% CO_2.

2.3. Animals

Male BALB/c mice (6 weeks old, 20−22 g) were purchased from the Laboratory Animal Center of Shanghai University of Traditional Chinese Medicine. Mice were kept under standard laboratory conditions with a 12 h light/dark cycle, humidity ranging from 60% to 70%, temperature maintained at 23−25 °C, and provided with free access to food and drinking water. All animal experiments were conducted in accordance with the principles of the declaration and recommendations of the Animal Experimentation Ethics Committee at Shanghai University of Traditional Chinese Medicine (Approval Number: PZSHU9TCM210604006; PZSHUTCM200828001; PZSHUTCM200724008).

2.4. Establishment of a CPT11-induced gut mucositis model in colorectal cancer xenograft mice

The animal model was established as described previously[25]. Briefly, CT26 cells (1×10^6 cells in 100 μL of phosphate buffer saline (PBS)) were harvested and subcutaneously injected into the right flank of mice. Three days later, all mice were randomly divided into four groups ($n = 6$−8 per group). Mice in the control group were administrated an oral gavage of 0.5% sodium carboxymethylcellulose (CMC-Na, Sangon Biotech, China) on Days 3−14; the remaining three groups of mice were injected intraperitoneally with CPT11 (60 mg/kg) on Days 5−9. Mice in CPT11+DDIE (25 and 75 mg/kg) groups were also administered DDIE (25 or 75 mg/kg dissolved in 0.5% CMC-Na) by gavage on Days 3−14. Tumor volume was determined by measuring length (mm), width (mm), and applying Eq. (1):

$$\text{Volume} = \text{Length} \times \text{Width}^2/2 \quad (1)$$

Body weight was measured daily, and the mice were sacrificed on Day 14. Blood was collected from the eye orbits of mice, which were anesthetized with isoflurane prior to the procedure. The entire colon and the solid tumors were removed and separated, and the total length of the colon and the weight of tumors were measured. Then, the feces were collected from the rectum.

2.5. Fecal microbiota transplantation (FMT) experiment

FMT was performed according to an established protocol[26]. In brief, stools (50 mg) from CPT11- or CPT11+DDIE-treated mice were collected and suspended in 600 μL of sterile saline. The solution was vigorously vortexed for 10 min and centrifuged at 587 × *g* for 1 min. The supernatant was collected for transplantation. The transplant material was obtained on the day of the transplantation.

Mice were randomly divided into two groups: CPT11-FMT group and DDIE-FMT group ($n = 6$). All mice were orally gavaged with 0.2 mL of an antibiotic (ABX) cocktail (1 g/L ampicillin, 0.5 g/L neomycin, 0.5 g/L vancomycin, and 1 g/L metronidazole) for 3 consecutive days after 6 h fast. All mice were injected intraperitoneally with CPT11 (60 mg/kg) on Days 3−9, and transplantation was performed by oral gavage of 200 μL of corresponding fecal bacteria on Days 1−13. The mice were closely observed for activity, and body weight was measured daily.

2.6. Bacterial cultivation and colonization experiment

E. faecalis (*E. faecalis*, Ningbo Testobio Co., Ltd., China) was cultured in brain heart infusion broth (Coolaber, China) at 37 °C. *E. faecalis* was adjusted to an optical density of 0.25 at 600 nm (OD_{600}) (∼10^8 colony-forming unit (CFU)/mL) and inoculated into fresh brain heart infusion broth at a ratio of 1:50.

Male BALB/c mice were randomly divided into three groups ($n = 6$). All mice received an oral gavage of 0.2 mL of an antibiotic cocktail for 3 consecutive days. All mice were intraperitoneally injected with CPT11 (60 mg/kg) from Days 3−9. In the CPT11+*E. faecalis* group, mice were orally gavaged with 10^8

CFU of *E. faecalis* in 200 μL of normal saline from Days 1−13. In the CPT11+*E. faecalis*+ABX group, mice were orally gavaged with 10^8 CFU of *E. faecalis*, pre-inactivated with ABX, from Days 1−13. Daily monitoring of mouse activity and regular measurement of body weight were conducted throughout the study period.

2.7. Histopathological evaluation

Colon tissues and tumors were immersed in 4% paraformaldehyde and then embedded in paraffin for hematoxylin and eosin (H&E) staining, or Alcian blue (AB) and Periodic Acid−Schiff (PAS) staining. The number of goblet cells was counted using ImageJ software (Media Cybernetics, MD, USA). Three fields of each section were randomly selected. Histopathological injury was evaluated as a combined score of inflammatory cell infiltration (score 0−3) and mucosal damage (score 0−3) according to the previous study[25].

2.8. Transmission electron microscopy (TEM)

Colon tissues of mice were removed and fixed with 2.5% glutaraldehyde. After being washed with PBS, the tissues were post-fixed with 1% osmium tetroxide at 4 °C for 2 h. Then, the samples were rinsed with PBS, and dehydrated with acetone. The samples were embedded in Embed-812 (Electron Microscopy Sciences, USA) and cured at 60 °C for 48 h. Ultrathin sections with a thickness of 50 nm were cut using a diamond knife on a ULTRACUT UC7 ultramicrotome (Leica, Germany) and stained with 4% uranyl acetate for 10 min and lead citrate for 8 min. Stained sections were scanned using a Hitachi HT7700 transmission electron microscope (Hitachi, Japan).

2.9. Intestinal permeability measurement

Intestinal permeability was measured as described previously[27]. Briefly, mice were fasted for 4 h and then orally gavaged with fluorescein isothiocyanate (FITC)−dextran (Sigma−Aldrich, CAS: 60842-46-8) at a concentration of 40 mg/100 g body weight 4 h before sacrifice. Serum was collected 4 h later, and the fluorescence intensity of each sample was measured by fluorometry at an excitation wavelength of 485 nm and an emission wavelength of 528 nm (Thermo Fisher Scientific, MA, USA).

2.10. Microbiota sequencing analysis

Total bacterial genomic DNA was extracted from feces using the E.Z.N.A. Soil DNA kit (Omega Bio-Tek, GA, USA), following the manufacturer's protocols. The quantity and quality of DNA were determined using the NanoDrop 2000 spectrophotometer (Thermo Fisher Scientific, USA). DNA degradation was identified by 1% (*w*/*v*) agarose gel electrophoresis. The V3−V4 hypervariable regions of bacterial 16S rRNA were amplified with specific primers (338F: 5′-ACTCCTACGGGAGGCAGCAG-3′ and 806R: 5′-GGACTACH VGGGTWTCTAAT-3′) using a thermocycler PCR system (GeneAmp 9700 PCR system, Carlsbad, CA, USA). Miseq library was generated using NEXTFLEX Rapid DNA Seq Kit (Bioo Scientific, Austin, Texas, USA) and sequenced using AxyPrep DNA Gel Extraction Kit (Corning, Shanghai, China). Operational taxonomic unit (OTU) were clustered with ≥97% sequence similarity cut-off using Uparse software (version 7.0.1090).

2.11. Immunofluorescence

Colon tissues were deparaffinized, rehydrated, and permeabilized in 0.1% Triton X-100 in PBS for 10 min at room temperature. The slides were incubated with blocking buffer (3% bovine serum albumin) for 30 min at room temperature. The primary antibodies ZO-1 (dilution 1:200), KLF4 (dilution 1:200), MUC2 (dilution 1:200), or KI67 (dilution 1:200) were incubated overnight at 4 °C, followed by incubation with secondary antibody (dilution 1:200) for 1 h at room temperature in the dark. Finally, the nuclei were stained with 4′,6-diamidino-2-phenylindole (DAPI) (Beyotime, Jiangsu, China). Samples were visualized under a fluorescence microscope (Olympus CKX41, Tokyo, Japan).

For immunofluorescence staining of organoids, the organoids were extracted from the matrix and fixed in pre-cooled 4% PFA for 45 min. After allowing the organoids to settle in suspension to remove PFA, they were washed once with PBS. Subsequently, permeabilization was performed using 1% Triton X-100 in PBS for 20 min at room temperature, followed by blocking with 1% bovine serum albumin in PBS for 1 h. Samples were then incubated overnight with primary antibodies against MUC2 (dilution 1:200) or KI67 (dilution 1:200). Following PBS washing, samples were incubated with the secondary antibody (dilution 1:200) for 1 h, washed again, stained with DAPI for nuclear visualization, and imaged using confocal microscopy.

2.12. Western blot analysis

Proteins were extracted from colon segments (1−1.5 cm) by homogenization in lysis buffer (Thermo Fisher Scientific, USA) containing protease and phosphatase inhibitor cocktail tablets (Roche Diagnostics GmbH, Mannheim, GER). The lysate was centrifuged (4 °C, 12,000 × *g*, 15 min), and the supernatant was collected. Proteins (30 μg) were separated by 10% or 12.5% sodium dodecyl sulfate polyacrylamide gel electrophoresis and transferred onto polyvinylidene fluoride membranes. The membranes were blocked with 5% (*w*/*v*) skim milk for 2 h at room temperature and incubated overnight with primary antibodies. The blots were washed and then incubated with an HRP-conjugated secondary antibody for 1 h at room temperature, followed by visualization using enhanced chemiluminescence detection. Protein expression levels were subsequently detected using a GS-700 imaging densitometer (Bio-Rad, Hercules, CA, USA), with β-actin used as internal control.

2.13. Reverse transcription quantitative polymerase chain reaction (RT-qPCR)

Total RNA was extracted using TRIzol Reagent (Life Technologies). Complementary DNA was synthesized using the *Evo M-MLV* RT Premix for qPCR (Accurate Biotechnology Co., Ltd., Chengdu, China). RT-qPCR was conducted using SYBR Green Premix × *Pro Taq* HS qPCR Kit (Accurate Biotechnology Co., Ltd., Chengdu, China) and quantitatively analyzed with the ABI Prism 7900HT Sequence Detection System (Life Technologies, Carlsbad, CA, USA). The thermal cycler was programmed with the following parameters: an initial denaturation at 95 °C for 30 s, followed by 40 cycles of denaturation at 95 °C for 5 s, and combined annealing/extension at 60 °C for 30 s. The comparative Ct method, with β-actin as the internal reference, was used to calculate gene expression changes. Primer sequences are listed in Supporting Information Table S1.

2.14. Enzyme-linked immunosorbent assay (ELISA)

Tumor necrosis factor (TNF)-α, interleukin (IL)-6, diamine oxidase (DAO), and lipopolysaccharide (LPS) levels in serum were determined using ELISA kits (Shanghai Yingxin Laboratory Equipment Co., Ltd., Shanghai, China) according to the manufacturer's instructions.

2.15. RNA sequencing

RNA was isolated from the intestinal tissues of mice using TRIzol reagent in strict adherence to the manufacturer's guidelines. The quality of the extracted RNA was assessed with a NanoDrop 2000 spectrophotometer (Thermo Fisher Scientific, USA). Subsequently, RNA sequencing libraries were prepared using the NEBNext Ultra RNA Library Prep Kit designed for Illumina sequencing. Sequencing was performed on an Illumina HiSeq platform. The analysis of differential gene expression was conducted using the cloud-based platform provided by Majorbio (https://cloud.majorbio.com/).

2.16. Fecal Gus activity and Gus-generating bacteria detection

Gus hydrolyzed 4-methylumbellifery-β-D-glucuronide (4-MUG, CAS: 6160-80-1, Shanghai Yuanye Bio-Technology Co., Ltd., Shanghai, China), producing fluorescence products, specifically 4-methylumbelliferone. Gus-producing bacteria were detected using an agar culture plate containing 4-MUG, as described previously[25]. Stools (50−70 mg) from each group were homogenized and centrifuged at 376 × *g* for 5 min. The fecal bacteria were then collected by centrifuging the supernatant at 9391 × *g* for 20 min and resuspended in 500 μL of PBS. The bacterial suspension was evenly smeared on the agar culture plate, and fluorescence intensities were detected under UV light at 366 nm after incubation for 12 h at 37 °C.

Fecal Gus activity was assessed by 4-nitrophenyl-β-D-glucopyranoside (PNPG) assay as described previously[25]. In brief, stool homogenate supernatant was quantified using the BCA Protein Assay Kit (Yeasen Biotechnology Co., Ltd., Shanghai, China). The reaction system consisted of 20 μL of protein, 20 μL of 0.5 mmol/L PNPG, and 80 μL of PBS. After incubation at 37 °C for 30 min, absorbance at 405 nm was measured.

2.17. Imaging of intestinal Gus activity

Mice (n = 3/group) were orally administered DDIE (75 mg/kg) or a matching volume of the vehicle control (200 μL of 0.5% CMC-Na) daily for three days. 30 min following the last dose of DDIE, the mice received an oral gavage of fluorescein di-β-D-glucuronide (FDGlcU, 7.3 μmol/kg, 0.1 mL per mouse) (CAS: 129787-66-2, BioRuler, CT, USA). Prior to the imaging process, the mice were euthanized, and imaging was performed using an IVIS Spectrum imaging system (Bruker, Germany) with 470 nm excitation and 535 nm emission filters.

2.18. Determination of CPT11 and SN38 content in feces

The concentrations of CPT11 and SN38 in mouse fecal samples were determined using the liquid chromatography−mass spectrometry (LC−MS) method as previously described[25]. For fecal sample processing, 40 mg of fecal material from each mouse was collected and mixed with 1 mL of acetonitrile. Homogenization was performed using a tissue grinder at 60 Hz for 60 s, followed by centrifugation at 18,000 × *g* for 5 min. The supernatant (500 μL) was then evaporated under nitrogen at 30 °C and reconstituted with 500 μL of methanol containing voriconazole (100 ng/mL). Subsequently, the Agilent® 1100 LC−MS system was employed for analysis, utilizing an Acquity UPLC® HSS T3 column (2.1 mm × 100 mm) with a gradient elution program. The mobile phases consisted of 0.1% formic acid aqueous solution (A) and 100% acetonitrile (B). An injection volume of 10 μL and a flow rate of 0.4 mL/min was used at a column temperature of 60 °C. The gradient elution was performed as follows: 30% B → 75% B (0−0.5 min), 75% B → 80% B (0.5−6 min), 80% B → 90% B (6−7 min), and 30% B (7−10 min). The API 5500−Qtrap triple quadrupole mass spectrometer, equipped with a Turbospray TM ion source, operated in electrospray ionization and multiple reaction monitoring scan modes for data acquisition.

2.19. Partial least squares path modeling (PLS-PM) analysis

We developed an optimized PLS-PM algorithm model by integrating methodologies from Qi et al.[28], using the 'plsmp' package in R. This model aimed to quantify the effects of various factors on DDIE's intervention in CPT11 treatment. The considered factors encompassed bacterial diversity (indicated by the Shannon and Simpson indices), potential probiotics (represented by *g_Alistipes* and *g_Roseburia*), epithelial regeneration (signified by *Muc2* and leucine-rich repeat-containing G-protein-coupled receptor 5 (*Lgr5*)), and the abundance of *E. faecalis* as determined from mouse fecal RT-qPCR results.

2.20. Antibacterial activity assay

To investigate the antibacterial effect of DDIE on *E. faecalis*, the final density of *E. faecalis* was adjusted to OD_{600} = 0.001. DDIE at final concentrations of 0, 50, 100, and 200 μmol/L was then added. Subsequently, OD_{600} values were measured at 0, 2, 4, 6, 8, and 12 h, respectively.

2.21. Isolation and culture of intestinal organoids

The colon tissues of mice were rinsed with PBS and finely diced. The diced tissue was then placed in a centrifuge tube and washed multiple times with PBS to remove debris. Subsequently, the tissue underwent ethylene diamine tetraacetic acid digestion on ice for organoid dissociation. Clean organoids were obtained after centrifugation. To culture the organoids, they were resuspended in Dulbecco's modified Eagle's medium/F-12, mixed with Matrigel Matrix (Corning, China), and pipetted into 24-well plates. Complete IntestiCult™ Organoid Growth Medium (Stemcell Technologies, Canada) was added to each well, and the culture medium was exchanged 3 times per week.

Organoids were treated with SN38G (100 nmol/L), SN38G (100 nmol/L) + *E. faecalis* (10^6 CFU), or SN38G (100 nmol/L) + *E. faecalis* (10^6 CFU) + DDIE (15 μmol/L) for 6 h on Day 2 of culture. Using an inverted microscope (Olympus, Tokyo, Japan), random images of organoids from each group were captured, and the surface area of organoids was measured using automated ImageJ software. To assess organoid-forming efficiency, the number of organoids formed on Day 6 of culture was counted in the same field of view.

2.22. Statistics

The data were presented as the mean ± standard deviation (SD) or standard error of the mean (SEM) and analyzed using GraphPad Prism 9.0 (GraphPad Software, La Jolla, CA, USA). Statistical comparisons between groups were analyzed by unpaired Student's *t*-test, Wilcoxon rank-sum test, or one-way analysis of variance (ANOVA). Spearman correlation analysis was performed to examine correlation relationships. The clinical data were sourced from the study conducted by Mahdy et al.[29]. A *P*-value less than 0.05 is considered statistically significant. The corresponding statistical difference is denoted as follows: $^{\#/}*P < 0.05$, $^{\#\#/}**P < 0.01$, $^{\#\#\#/}***P < 0.001$; 'ns' indicates not significant difference ($P > 0.05$).

3. Results

3.1. DDIE alleviated CPT11-induced gut mucositis in mice

The CPT11-induced gut mucositis model was established as described previously[25] (Fig. 1B). Intraperitoneal injection of CPT11 (60 mg/kg/day) for 5 consecutive days resulted in significant body weight loss and persistent diarrhea (Fig. 1C−E). Administration of DDIE (25 and 75 mg/kg) remarkably mitigated the weight loss and diarrhea in mucositis mice. Colon shortening serves as an indirect indicator of mucosal inflammation[25,30]. As expected, CPT11 treatment led to significant colon shortening, while oral administration of DDIE ameliorated colon shortening in mucositis mice (Fig. 1F and G).

Histological examination of colon tissue from mice exposed to CPT11 showed obvious histopathological changes, including neutrophil infiltration, disrupted epithelial structure, and crypt loss (Fig. 1H and I). In contrast, DDIE treatment exhibited less mucosal architecture loss and less inflammatory cellular infiltration. Since the high dose of DDIE (75 mg/kg) showed superior effects, the 75 mg/kg treatment group was selected for further experimental analyses.

Furthermore, RT-qPCR assay demonstrated that DDIE treatment significantly reduced the elevated mRNA levels of pro-inflammatory mediators *Cox-2*, *Il-6*, and *Tnf-α* in colon tissue in mucositis mice (Supporting Information Fig. S1A). The same trend was observed in the serum levels of IL-6 and TNF-α by ELISA assay (Fig. S1B). Consistently, increased protein levels of iNOS and COX-2 in the CPT11 group were reversed by DDIE treatment (Fig. S1C and S1D).

The above results indicate that DDIE effectively ameliorates CPT11-induced mucositis.

3.2. DDIE protected the integrity of the intestinal barrier in mice exposed to CPT11

CPT11-induced gut mucositis is associated with the disruption of tight junctions in the intestinal epithelium[4]. To evaluate the impact of DDIE on the intestinal epithelium, we examined specific indicators related to the integrity of the intestinal barrier. In the FITC-dextran fluorescence assay, mice exposed to CPT11 exhibited elevated FITC-dextran level compared to the control group, indicating increased permeability or disruption of the intestinal barrier (Fig. 2A). Conversely, mice treated with DDIE showed a decreased FITC-dextran level, suggesting a potential protective effect of DDIE against the compromised integrity induced by CPT11.

DAO and LPS are well-accepted serum biomarkers reflecting the integrity of the intestinal barrier[31]. ELISA assay revealed a significant elevation in serum levels of DAO and LPS in the CPT11 group (Fig. 2B), indicative of impaired intestinal barrier function. However, administration of DDIE led to a notable reduction in both DAO and LPS levels, signifying a restoration of intestinal barrier function.

Next, we assessed the gene expression levels of tight junction proteins (*Zo-1*, Claudin-7, and Occludin) in colon tissue. As depicted in Fig. 2C−E, the expression levels of mRNA (*Zo-1*, Claudin-7, Occludin) and proteins (Occludin, ZO-1) demonstrated a notable decline in the CPT11 group compared to the control group. Conversely, the DDIE treatment group manifested a significant enhancement in tight junction proteins relative to the CPT11 group. These results were further supported by immunofluorescence staining for the expression of ZO-1 in colon tissue, which demonstrated a consistent trend (Fig. 2F and G). Subsequently, colon tissue of mice was imaged by transmission electron microscopy, revealing that DDIE treatment effectively ameliorated the structural damage, shortening of intestinal villi, and loss of tight cell connections caused by CPT11 (Fig. 2H).

In vitro, the impacts of DDIE on the viability of NCM460 normal human intestinal epithelial cells were evaluated using the Cell Counting Kit-8 (CCK-8) assay. DDIE did not exhibit any cytotoxic effects within the tested concentration range of 30 μmol/L (Supporting Information Fig. S2A). The transepithelial electrical resistance experiment revealed that DDIE significantly mitigated the decrease in intestinal epithelial cell resistance induced by SN38 (Fig. S2B). Furthermore, the scratch wound healing assay showed that DDIE facilitated the healing of cell wounds caused by SN38 (Fig. S2C). Additionally, flow cytometry analysis revealed that DDIE effectively inhibited SN38-induced intestinal epithelial cell apoptosis (Fig. S2D).

Collectively, these data indicate that DDIE mitigates CPT11-induced mucositis, possibly by enhancing intestinal barrier integrity and facilitating wound healing.

3.3. DDIE improved intestinal epithelial differentiation in mice exposed to CPT11

To further investigate the mechanism of DDIE in CPT11-induced mucositis, we conducted transcriptomic analysis on mouse colorectal tissue using RNA sequencing. Principal component analysis (PCA) revealed significant differences in gene expression patterns between the control group and the CPT11 alone treatment group (Supporting Information Fig. S3A). Nevertheless, the close resemblance between the control group and the CPT11+DDIE group suggests that the administration of DDIE may alleviate the gene structure deviations induced by CPT11.

Subsequently, the volcano plot analysis of differential genes between the CPT11 and CPT11+DDIE groups unveiled a total of 1178 significantly different genes, comprising 380 up-regulated genes and 798 down-regulated genes (Fig. S3B). Gene Ontology (GO) enrichment analysis was then conducted on the differentially expressed genes, revealing the enrichment of several genes associated with inflammatory signaling functions, such as cellular response to interferon-beta, negative regulation of inflammatory response, response to interferon-beta, and granulocyte chemotaxis (Fig. 3A). Additionally, there was an enrichment of signaling pathways linked to intestinal epithelium, including epidermis

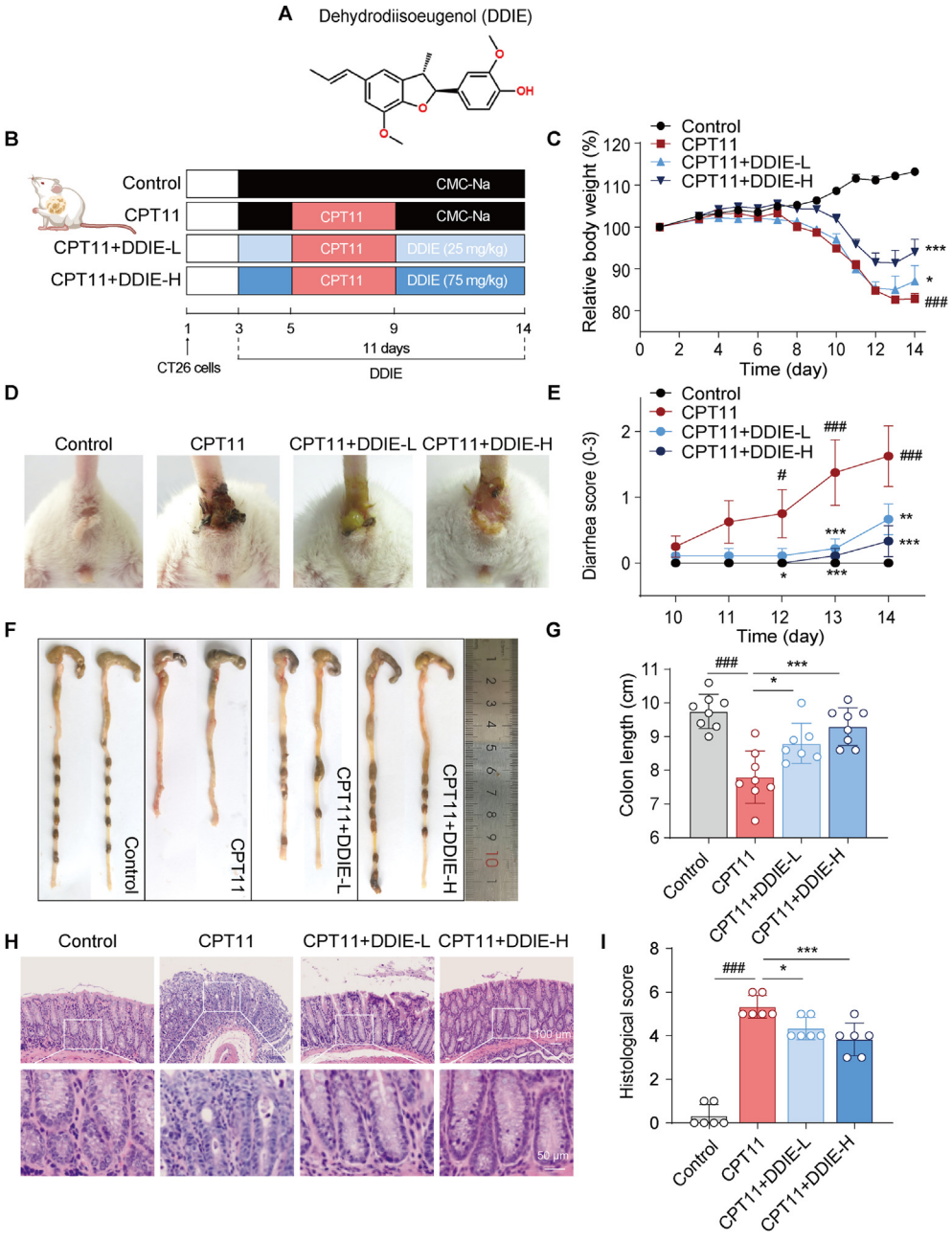

Figure 1 DDIE alleviated the intestinal toxicity induced by CPT11 in colorectal tumor xenograft mice. (A) Chemical structure of DDIE. (B) Schematic diagram of the experimental procedure. (C) Body weight was recorded following the animal experiment. Data were plotted as a percentage of basal body weight. Data are expressed as mean ± SEM (n = 6−8). (D) The representative anus photographs. (E) Diarrhea scores were evaluated as described in Methods. Data are expressed as mean ± SEM (n = 6−8). (F, G) The representative colon was photographed and colon length was measured (n = 6). (H, I) The representative colon H&E staining and histopathological scores analysis (n = 6). Data are expressed as mean ± SD. $^{\#}P < 0.05$, $^{\#\#\#}P < 0.001$ *vs.* Control group; $^{*}P < 0.05$, $^{**}P < 0.01$, and $^{***}P < 0.001$ *vs.* CPT11 group.

development, regulation of epithelial cell differentiation, and keratinocyte differentiation.

Given that the differentiation of ISCs into secretory-lineage cells, including goblet cells, tuft cells and Paneth cells, is crucial for maintaining the integrity of the intestinal epithelial barrier, subsequent heatmap analysis revealed a notable decrease in mRNA expression linked to stem cells, goblet cells, tuft cells, and Paneth cells following treatment with CPT11 (Fig. 3B). However, the administration of DDIE effectively reversed the abnormal reduction in the aforementioned mRNA levels observed in the CPT11-treated group. Furthermore, RT-qPCR experiments provided additional confirmation that DDIE significantly increased the mRNA expression related to stem cells (*Lgr5*, polycomb ring finger (*Bmi1*), and achaete-scute family bHLH transcription factor 2 (*Ascl2*)) and goblet cells (*Klf4*, protease-resistant trefoil factor 3 (*Tff3*), and *Muc2*). Additionally, DDIE also elevated the mRNA expression related to tuft cells (doublecortin-like kinase 1 (*Dclk1*), transient receptor potential channel subfamily M member 5 (*Trpm5*)) and Paneth cells (*β*-defensin1, *β*-defensin2, and lysozyme (*Lyz1*)), although the differences were not statistically

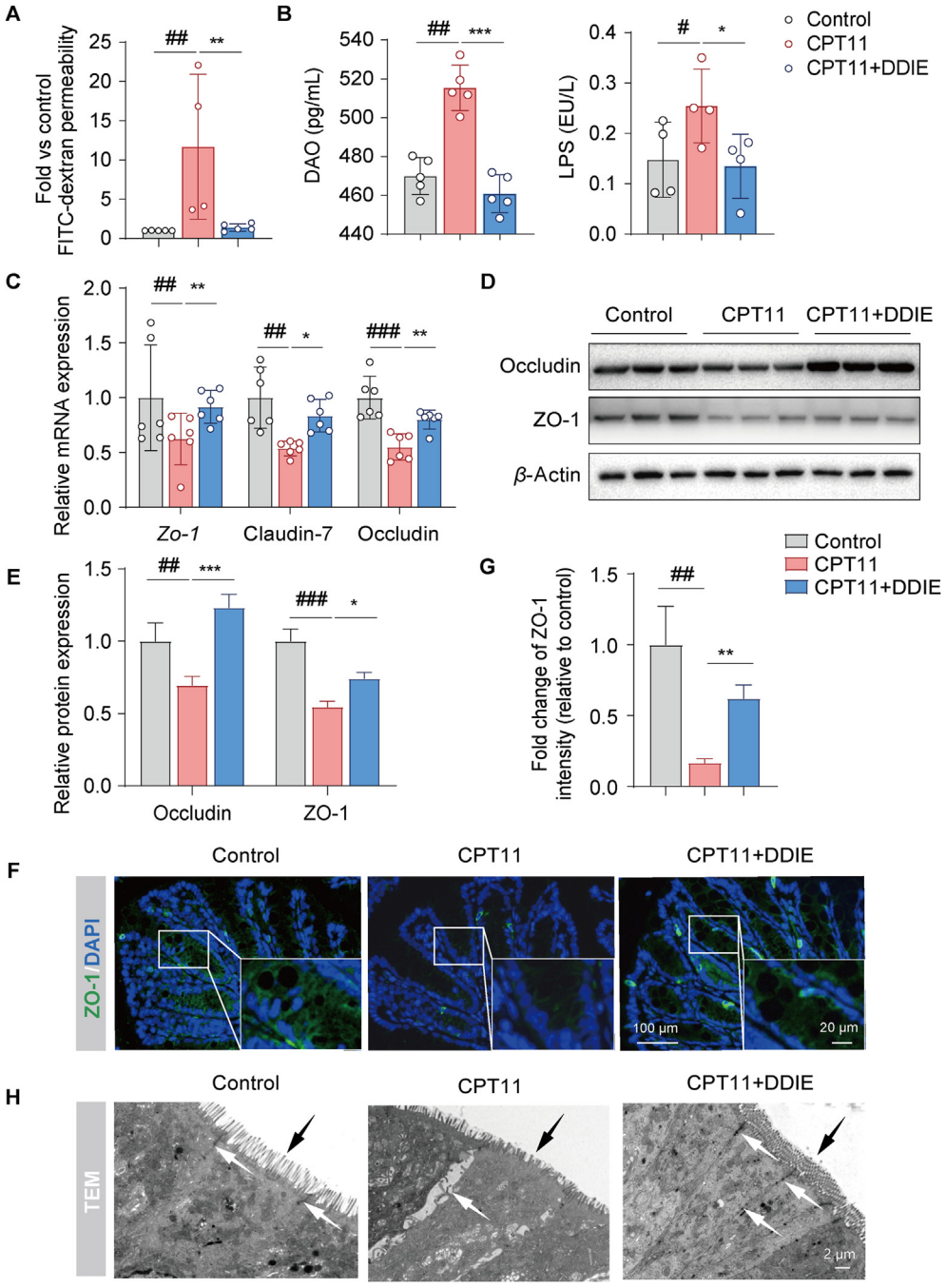

Figure 2 DDIE protected against the intestinal barrier disruption induced by CPT11. (A) Serum concentrations of FITC-dextran and (B) DAO and LPS levels in mice (n = 4−5). (C) The relative mRNA levels of the *Zo-1*, Claudin-7, and Occludin in colon tissues across each group (n = 6). (D, E) Representative Western blots and quantitative analysis of Occludin and ZO-1 in colon tissues (n = 3). (F, G) Representative immunofluorescence images and quantification of ZO-1 (green) in colon tissues (n = 3). Nuclei were labeled with DAPI (blue). (H) Representative transmission electron microscopy (TEM) images of colon tissues (white arrows: tight junctions between cells; black arrows: villi). Data are expressed as mean ± SD. $^{\#}P < 0.05$, $^{\#\#}P < 0.01$, and $^{\#\#\#}P < 0.001$ *vs.* Control group; $^{*}P < 0.05$, $^{**}P < 0.01$, and $^{***}P < 0.001$ *vs.* CPT11 group.

significant (Fig. 3C). These findings indicate the promotional effect of DDIE on the self-renewal of damaged intestinal epithelium in mice with CPT11-induced mucositis.

Goblet cells, serving as pivotal mucus-secreting entities, play a crucial role in maintaining mucosal barrier function[32,33]. To further assess the impact of DDIE on mucus secretion in CPT11-treated mice, we quantified the number of goblet cells and assessed the level of mucus-like glycoprotein in the colon using AB-PAS staining. As illustrated in Fig. 3D−F, mice exposed to CPT11 exhibited a noteworthy decrease in goblet cell numbers and a reduced level of mucus-like glycoprotein compared to the control group. In contrast, DDIE treatment significantly

increased the number of goblet cells and elevated mucin-like glycoprotein levels. Transmission electron microscopy of colon tissue further revealed the restoration of goblet cells following DDIE administration (Fig. 3G). Immunofluorescent staining demonstrated elevated levels of the cell proliferation marker (KI67), goblet cell mucin-related protein (MUC2), and goblet cell-specific differentiation protein (KLF4) in the colons of mice co-treated with DDIE compared to those treated with CPT11 alone (Fig. 3H and I). Western blot analysis further confirmed these trends (Fig. S3C).

These data indicate that DDIE improves intestinal barrier integrity in CPT11-induced mucositis mice, at least partly, by enhancing intestinal epithelial differentiation.

3.4. *DDIE suppressed intestinal Gus-producing bacteria and reduced Gus activity in mice exposed to CPT11*

The gut microbiota plays a crucial role in digestion, nutrient absorption, immune system development, and protection against pathogens. Maintaining a balance and diversity in the microbiota is essential for immune homeostasis and disease prevention[33]. High-throughput sequencing of the V3−V4 regions of the 16S rRNA gene in colonic contents was conducted to investigate whether DDIE treatment modifies the gut microbiota in CPT11-induced mucositis mice. Principal coordinates analysis (PCoA) revealed that the microbiota composition of the CPT11 group significantly differed from that of the control group, while the DDIE group exhibited a trend of deviation towards the control group (Fig. 4A).

Subsequently, we employed the Simpson index and Shannon index to assess microbial diversity. Both metrics indicated a noteworthy decrease in bacterial diversity in the CPT11 group compared to the control group, whereas the administration of DDIE led to a notable increase in bacterial diversity (Fig. 4B and C). The major microbiota at the phylum level were identified as Bacteroidota, Firmicutes, Proteobacteria, and Verrucomicrobia (Fig. 4D, Table S2). Notably, CPT11 administration had a negative impact on the relative abundance of Bacteroidota compared to the control group, while it had a positive impact on the relative abundance of Proteobacteria, Actinobacteriota, and Verrucomicrobia (Fig. 4D, Table S2). However, upon administering DDIE, the abundance of Bacteroidota increased, and that of Actinobacteriota decreased.

The intestinal toxicity caused by CPT11 is attributed to the accumulation of SN38 in the GI tract, with the Gus enzyme playing a crucial role as a key driver in converting inactive SN38G to active SN38 in the intestinal lumen[29]. Consequently, we propose that regulating Gus-producing bacteria might constitute the primary mechanism through which DDIE alleviates CPT11-induced mucositis. To investigate this hypothesis, we conducted an analysis of the abundance of Gus-producing bacteria (*g_Bacteroides*, *g_Alistipes,* *g_Parabacteroides*, *g_Prevotella*, *g_Anaerotruncus*, *g_Blautia*, *g_Enterococcus*, *g_Lactobacillus,* and *g_Roseburia*) using 16S rRNA sequencing (Table S2). Fig. 4E clearly depicts a significant increase in the total abundance of Gus-producing bacteria after CPT11 treatment. In contrast, in the DDIE co-treated group, the total abundance of Gus-producing bacteria decreased compared to the CPT11 group. A detailed analysis of the relative abundance of various bacterial genera revealed that CPT11 treatment notably reduced the abundance of *g_Alistipes*, while concurrently increasing that of *g_Enterococcus* (Fig. 4F). Conversely, following DDIE administration, the abundance of *g_Enterococcus* markedly decreased, while the abundance of *g_Roseburia* significantly increased.

By establishing a mouse fecal Gus-generating bacteria and Gus activity detection system (Fig. 4G), we employed 4-MUG agar to assess the activity of Gus-producing bacteria in fecal samples, following a previously described method[25]. As anticipated, the fluorescence intensity increased after CPT11 exposure, indicating a higher presence of Gus-producing bacteria in the fecal samples of the CPT11 group (Fig. 4H). In contrast, the fluorescence intensity in the CPT11+DDIE group was comparable to that of the control group, suggesting that DDIE treatment decreased Gus-producing bacteria.

Based on the aforementioned findings, the subsequent objective was to investigate whether DDIE directly inhibits Gus activity. Gus activity in mouse feces was assessed using the PNPG assay[13]. The CPT11 group demonstrated a notable increase in Gus activity compared to the control group, whereas the administration of DDIE led to a significant reduction in Gus activity (Fig. 4I). Additionally, we conducted *in vivo* imaging of mice orally administered with FDGlcU, utilizing fluorescence intensity as an indicator of Gus activity[12]. The results depicted in Fig. 4J show an amplified fluorescence signal in the CPT11 group compared to the control group, while the DDIE treatment group displayed a diminished fluorescence signal. Moreover, functional prediction utilizing the Fax4Fun software, based on 16S rRNA sequencing data, revealed an enrichment of Gus orthology (Description: beta-glucuronidase [EC: 3.2.1.31])[34] in the CPT11 group (Supporting Information Fig. S4A). Conversely, the DDIE group exhibited a significant reduction in this orthology compared to the CPT11 group. These findings strongly suggest that DDIE inhibits Gus enzyme activity.

Molecular docking analysis was further performed to predict the affinity between DDIE and *Enterococcus coli* Gus. The results indicated that amino acid residues ARG71 and GLN72 could form hydrogen bonds with DDIE, resulting in a binding energy of −6.56 kcal/mol (Fig. S4B). Notably, this binding energy was comparable to that of a known Gus enzyme inhibitor with a value of −8.6 kcal/mol. Subsequent enzyme activity assay demonstrated dose-dependent inhibitory effect of DDIE on Gus activity (Fig. S4C). These findings suggest that while DDIE may prevent the increase of Gus-producing bacteria induced by CPT11, it has relatively weak direct inhibition on Gus itself.

Subsequently, LC−MS analysis was conducted to determine the fecal content of CPT11 and SN38 in mice. The results revealed a non-significant decrease in CPT11 levels in feces following DDIE administration compared to the CPT11 group (Fig. 4K). However, a notable reduction in SN38 levels was observed in the feces of the DDIE-treated group in comparison to the CPT11 group, indicating DDIE decreases SN38 concentration in the intestinal lumen.

Collectively, these data indicate that DDIE decreases colorectal content of SN38 through suppressing the increased total Gus-generating bacteria and reducing the Gus enzyme activity in CPT11 mucositis mice.

3.5. *The mitigation of CPT11-induced mucositis by DDIE was gut microbiota dependent*

In order to verify the contribution of the gut microbiota to the alleviation of CPT11-induced mucositis by DDIE, FMT experiments were conducted. Briefly, fecal microbiota from mice treated with CPT11 or DDIE was transplanted into recipient mice with

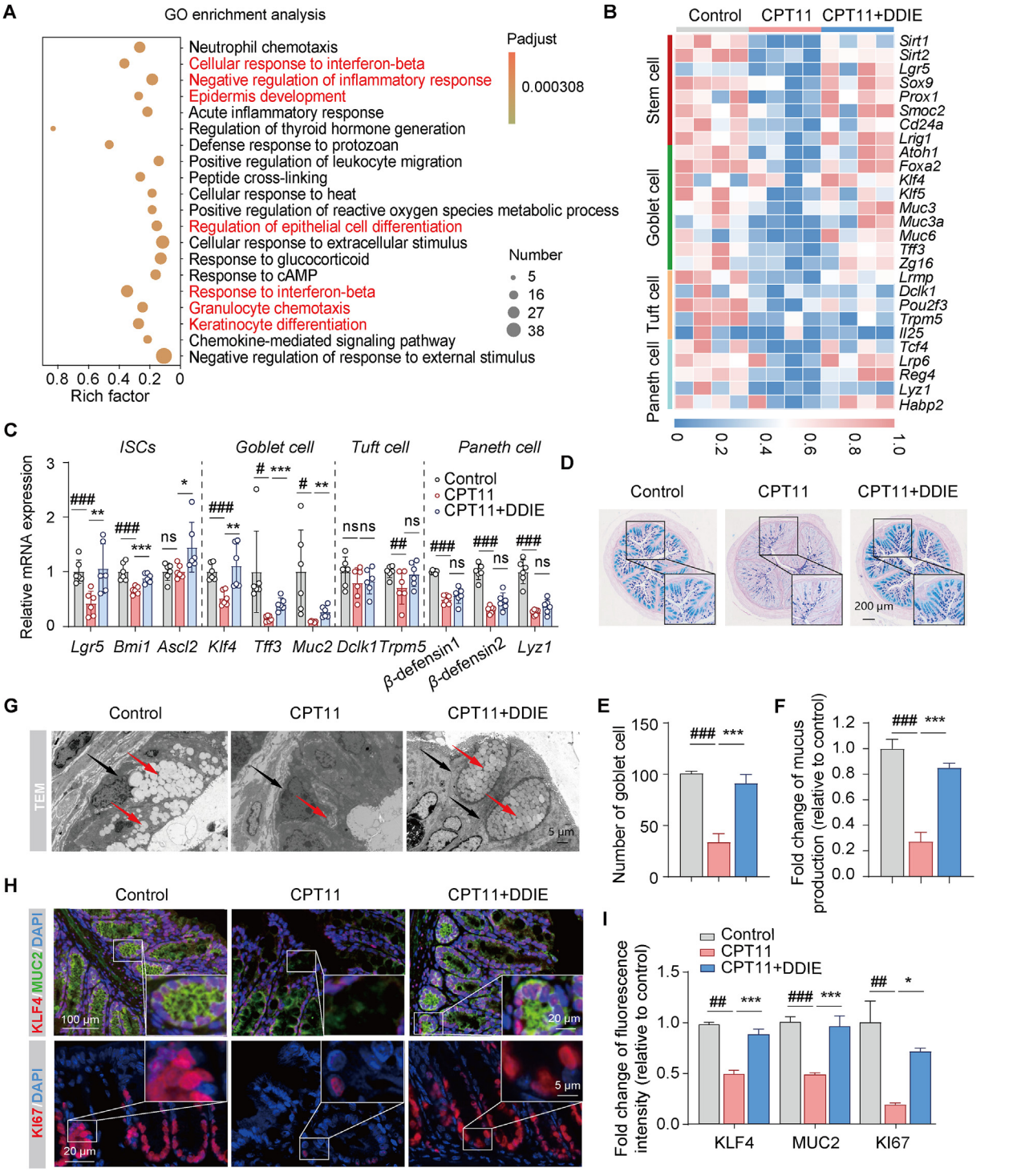

Figure 3 DDIE promoted intestinal epithelial differentiation in CPT11-induced mucositis mice. (A) GO enrichment analysis on differentially expressed genes between the CPT11 group and the CPT11+DDIE group. The color intensity represents the adjusted *P*-value, and the node size reflects the number of genes in that category ($n = 4$). (B) Heatmap analysis of expression patterns of marker genes for stem cells, goblet cells, tuft cells and Paneth cells ($n = 4$). (C) mRNA levels of *Lgr5*, *Bmi1*, *Ascl2*, *Klf4*, *Tff3*, *Muc2, Dclk1*, *Trpm5*, β-defensin1, β-defensin2, and *Lyz1* in ISCs and secretory-lineage cells in colon tissues ($n = 6$). (D) Representative AB-PAS staining of colonic sections and (E) the counting of goblet cells per villus calculation unit ($n = 3$). (F) Assessment of mucus production ($n = 3$). (G) Representative images of TEM of colon tissues (red arrows: mucin particles, black arrows: goblet cells). (H, I) Representative immunofluorescence images and qualification of KLF4 (red), MUC2 (green), and KI67 (red) in colon tissues ($n = 3$). Nuclei were labeled with DAPI (blue). Data are expressed as mean ± SD. $^{\#}P < 0.05$, $^{\#\#}P < 0.01$, and $^{\#\#\#}P < 0.001$ *vs.* Control group; $^{*}P < 0.05$, $^{**}P < 0.01$, and $^{***}P < 0.001$ *vs.* CPT11 group. ns, not significant.

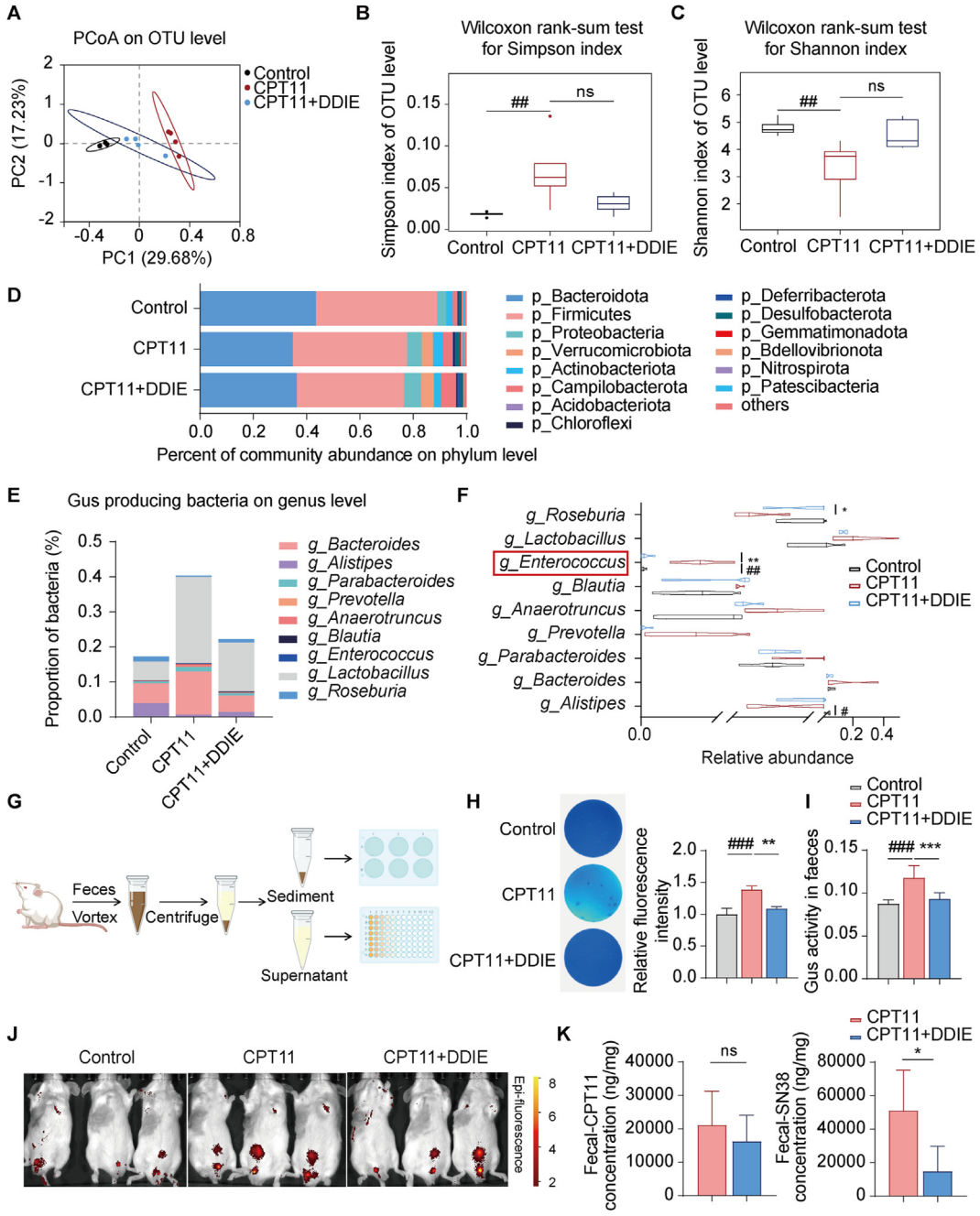

Figure 4 DDIE reshaped the gut microbiota, suppressed Gus-generating microbiota, and reduced Gus activity in mice exposed to CPT11. (A) Principal coordinates analysis (PCoA) of Control (black dots), CPT11 (red dots) and CPT11+DDIE (blue dots) samples at the OTU level ($n = 4$). (B) Alpha diversity of fecal microbiota profiles calculated using the Simpson index at the OTU level. Data are presented as median with interquartile range with whiskers extending from minimum to maximum. Statistical significance determined by Wilcoxon rank-sum test ($n = 4$). (C) Alpha diversity of fecal microbiota profiles calculated using the Shannon index at the OUT level. Data are presented as median with interquartile range with whiskers extending from minimum to maximum. Statistical significance determined by Wilcoxon rank-sum test ($n = 4$). (D) Percent of community abundance of differentially expressed bacteria at dominant phyla level in fecal microbiota across the different group ($n = 4$). (E) Stacked bar chart of the proportion of Gus-producing bacteria at the genus level in fecal microbiota ($n = 4$). Each bar represents a distinct group of fecal samples, with segments indicating the relative abundance of various Gus-producing bacterial genera. (F) The violin plots display the distribution of Gus-producing bacteria at the genus level in different groups of fecal samples, with lines within each violin representing the median ($n = 4$). (G) Schematic diagram of the fecal Gus detection procedure. (H) Representative images of Gus-producing bacteria in feces and analysis of relative fluorescence intensity. Bacteria were detected using an agar medium supplemented with 4-MUG ($n = 4$). The more intense the blue coloration, the greater the abundance of Gus-producing bacteria. (I) Gus activity in feces was detected by PNPG assay ($n = 4$). (J) Intestinal Gus activity was visualized by *in vivo* imaging. Red to yellow Epi-fluorescence represents Gus activity from low to high. (K) The levels of CPT11 and SN38 in feces were detected by LC−MS ($n = 4$). Data are expressed as mean ± SD. $^{\#}P < 0.05$, $^{\#\#}P < 0.01$, and $^{\#\#\#}P < 0.001$ *vs.* Control group; $^{*}P < 0.05$, $^{**}P < 0.01$, and $^{***}P < 0.001$ *vs.* CPT11 group. ns, not significant.

CPT11-induced mucositis (Fig. 5A). As anticipated, mice administrated with DDIE fecal microbiota have a significantly increased body weight, decreased FITC-dextran level and a longer colon length compared to those were transplanted with CPT11 fecal microbiota (Fig. 5B−D). Correspondingly, the CPT11+DDIE-FMT group exhibited improved goblet cell mucus-secretion and mitigated colonic pathology relative to the CPT11-FMT group (Fig. 5E and F).

Immunofluorescence staining in the DDIE-FMT group indicated a substantial upregulation of genes related to goblet cell differentiation and function (KLF4, MUC2) compared to the CPT11-FMT group (Fig. 5G). 4-MUG and PNPG assays indicated that fecal bacteria from DDIE-treated mice significantly reduced the presence of Gus-producing bacteria and intestinal Gus activity in mice, respectively (Fig. 5H and I). Additionally, according to the aforementioned data, the Gus-generating bacterium, *g_Enterococcus* was increased in the colon of CPT11-exposed mice (Fig. 4F). We therefore assessed the abundance of *g_Enterococcus* and the representative species, *E. faecalis* and *Enterococcus faecium,* in mouse feces by RT-qPCR. The results showed that in the CPT11+DDIE-FMT group, the abundance of *g_Enterococcus* and *E. faecalis* was significantly reduced compared to the CPT11-FMT group (Fig. 5J). However, there were no significant changes in the abundance of *E. faecium*.

To explore whether DDIE retains its capability to alleviate CPT11-induced intestinal mucosal damage in the absence of gut microbiota, a pseudo-germ-free mouse model was established through antibiotic administration to deplete the gut microbiota (Supporting Information Fig. S5A). A significant increase in body weight in mice from the 3rd day of DDIE treatment was observed (Fig. S5B). However, by the 5th day of CPT11 modeling, the difference in body weight between the two groups was not statistically significant. Additionally, the FITC-dextran experiment showed no significant difference in serum FITC-dextran levels between the groups (Fig. S5C). Moreover, assessments, including colon length measurements, histopathological scoring, and goblet cell counts, indicated no significant changes between the groups (Fig. S5D−S5F).

These data indicate that the improved effects of DDIE against CPT11-induced intestinal toxicity rely on the presence of gut microbiota.

3.6. Targeted inhibition of the Gus-generating bacterial strain E. faecalis contributed significantly to the anti-mucositis of DDIE by promoting intestinal epithelial differentiation

To delve deeper into the role of key microbial players, we conducted a correlation analysis between Gus-producing microbes and various disease markers in mice. The results indicated notable positive associations between the abundance of *g_Bacteroides* or *g_Enterococcus* and indicators of intestinal inflammation (mRNA of *Cox-2* and *Il-6*), along with markers linked to intestinal permeability (FITC-dextran) (Fig. 6A). Moreover, *g_Enterococcus* exhibited notable negative correlations with indicators associated with intestinal tight junctions (mRNA of *Zo-1*, Claudin-7, and Occludin), ISCs (mRNA of *Lgr5* and *Bmi1*), and goblet cells (mRNA of *Klf4*).

Subsequent RT-qPCR analysis confirmed the increased abundance of *g_Bacteroides, g_Parabacteroides,* and *g_Enterococcus* in the feces of the CPT11 group, while DDIE effectively attenuated this trend (Fig. 6B). Notably, the relative fold amplification of *g_Enterococcus* was more pronounced compared to that of *g_Bacteroides*. These results highlight the specific impact of DDIE on modulating the gut microbiota composition, particularly in reducing the abundance of *g_Enterococcus*, which may contribute to its attenuating effects against CPT11-induced mucositis.

Next, we further analyzed fecal 16S rRNA sequencing data from healthy individuals, patients with colorectal cancer undergoing CPT11 chemotherapy (CRC+CPT11), and those not receiving CPT11 chemotherapy (CRC). Gus functional predictions by Fax4Fun, based on the fecal 16S rRNA sequencing data, revealed an elevation in the relative abundance of fecal Gus in patients receiving CPT11 chemotherapy ($P = 0.9139$) (Fig. 6C). Moreover, an increased relative abundance of *g_Enterococcus* was observed in the fecal 16S rRNA sequencing data of patients undergoing CPT11 chemotherapy. This finding provides insights into the contributory role of *g_Enterococcus* in CPT11 chemotherapy GI toxicity.

According to the aforementioned FMT data with respect to the representative species within the genus *g_Enterococcus,* DDIE was indicated to most prominently influence the abundance of *E. faecalis* (Fig. 5J). Therefore, we established a PLS-PM to elucidate and quantify the intricate interrelations among microbial diversity (measured by Simpson and Shannon indices), potential probiotics (genera *Alistipes* and *Roseburia*), Gus-expressing bacterium (*E. faecalis*), and mucosal regeneration markers (*Lgr5*, *Muc2*). The results indicated that CPT11 exposure exhibited negative correlations with microbial diversity (−0.02), mucosal regeneration (−0.93), and the abundance of potential intestinal probiotics (−0.70), while displaying a positive correlation with the abundance of *E. faecalis* (0.69) (Fig. 6D). On the contrary, after treatment with DDIE, positive correlations were observed with microbial diversity (0.89), mucosal regeneration (0.58), and the abundance of potential intestinal probiotics (0.34). Furthermore, a significant negative correlation was noted with the abundance of *E. faecalis* (−0.80), indicating a significant shift in the microbial landscape and mucosal response (Fig. 6D). It is notable that the potential probiotic (0.91) positively influenced mucosal regeneration, while *E. faecalis* (−0.64) had a detrimental impact on intestinal mucosal regeneration and repair.

Subsequently, an *E. faecalis* colonization experiment was conducted to more precisely assess its impact on CPT11-induced intestinal mucositis (Fig. 7A). Mice orally administered with *E. faecalis* exhibited more severe intestinal mucositis compared to the CPT11 group, showing significant weight loss, exacerbated diarrhea, colon shortening, reduced goblet cells, and pathological damage in the colon tissue (Fig. 7B−F). In contrast, mice administered with antibiotic-treated *E. faecalis* did not display worsened intestinal mucositis compared to the CPT11 group. RT-qPCR analysis confirmed the heightened abundance of *E. faecalis* in the feces of mice in the CPT11+*E. faecalis* group (Fig. 7G). Subsequent 4-MUG and PNPG assays revealed an increased presence of Gus-producing bacteria and higher Gus activity in mouse feces following *E. faecalis* colonization (Fig. 7H).

To further explore the impact of *E. faecalis* on CPT11-induced crypt cell damage, we established an *in vitro* 3D crypt organoid model. Co-incubation of organoids with *E. faecalis* or SN38 led to a notable reduction in the organoid-forming efficiency and organoid surface area, along with decreased expression of the goblet cell marker MUC2 (Fig. S5G). However, the administration of antibiotics effectively mitigated the adverse effects of *E. faecalis*

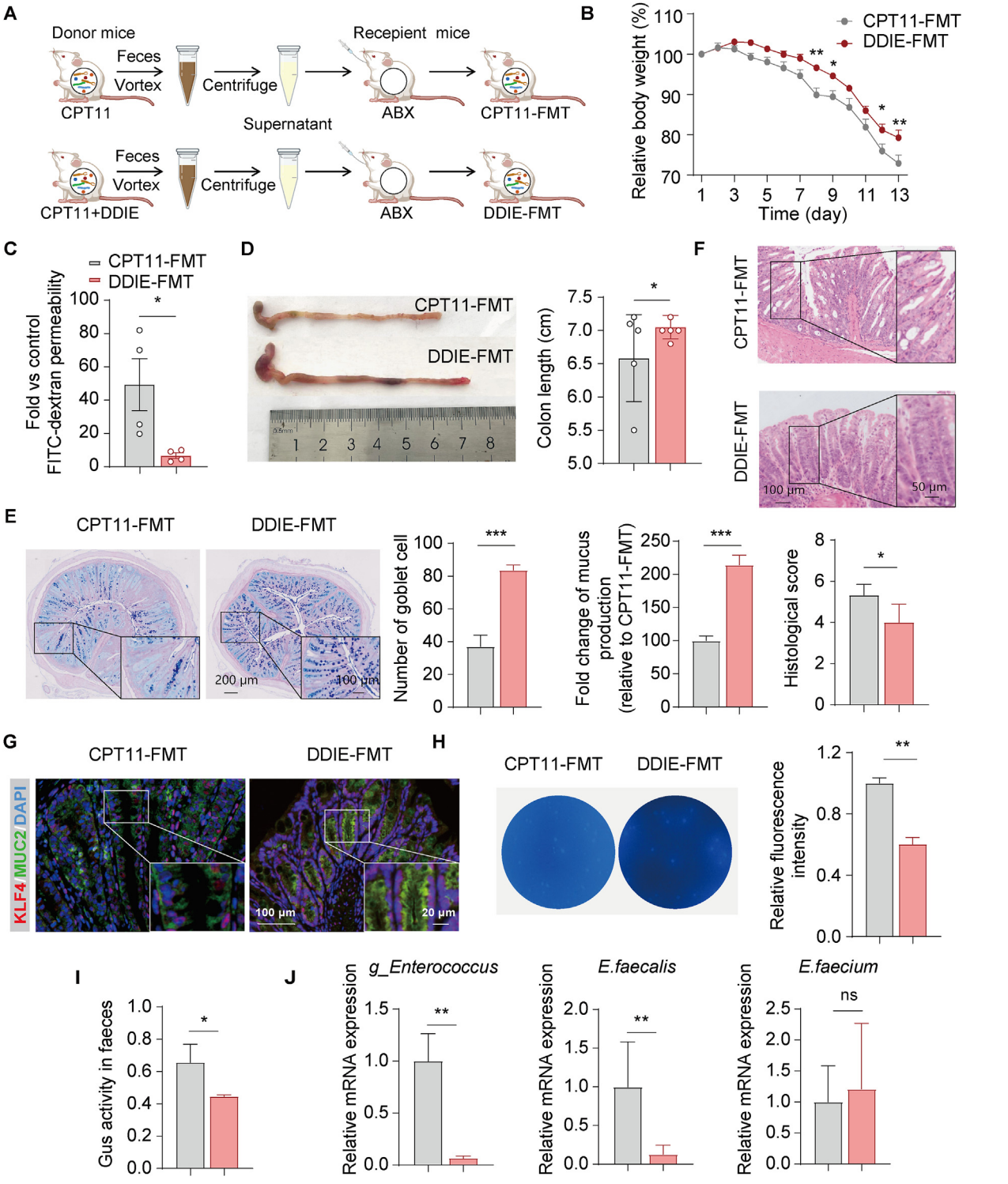

Figure 5 The gut microbiota-mediated mitigation of CPT11-induced intestinal mucositis by DDIE. (A) Schematic diagram of the experimental procedure. (B) Body weight was recorded following the animal experiment. Data were plotted as a percentage of basal body weight. Data are expressed as mean ± SEM ($n = 6$). (C) Serum concentrations of FITC-dextran in mice. Data are expressed as mean ± SEM ($n = 4$). (D) Representative colon photographs and colon length were measured ($n = 5$). (E) Representative AB-PAS staining of the colonic sections, the counting of goblet cells per villus calculation unit, and the assessment of mucus production ($n = 3$). (F) H&E staining sections and histopathological scores ($n = 3$). (G) Representative immunofluorescence images of KLF4 (red) and MUC2 (green) in colon sections. Nuclei were labeled with DAPI (blue). (H) Gus-producing bacteria in feces were detected by agar medium supplemented with 4-MUG ($n = 3$). (I) Gus activity in feces was detected by PNPG assay ($n = 3$). (J) mRNA levels of *g_Enterococcus*, *E. faecalis* and *E. faecium* in feces ($n = 6$). Data are expressed as mean ± SD. $^{*}P < 0.05$, $^{**}P < 0.01$, and $^{***}P < 0.001$. ns, not significant.

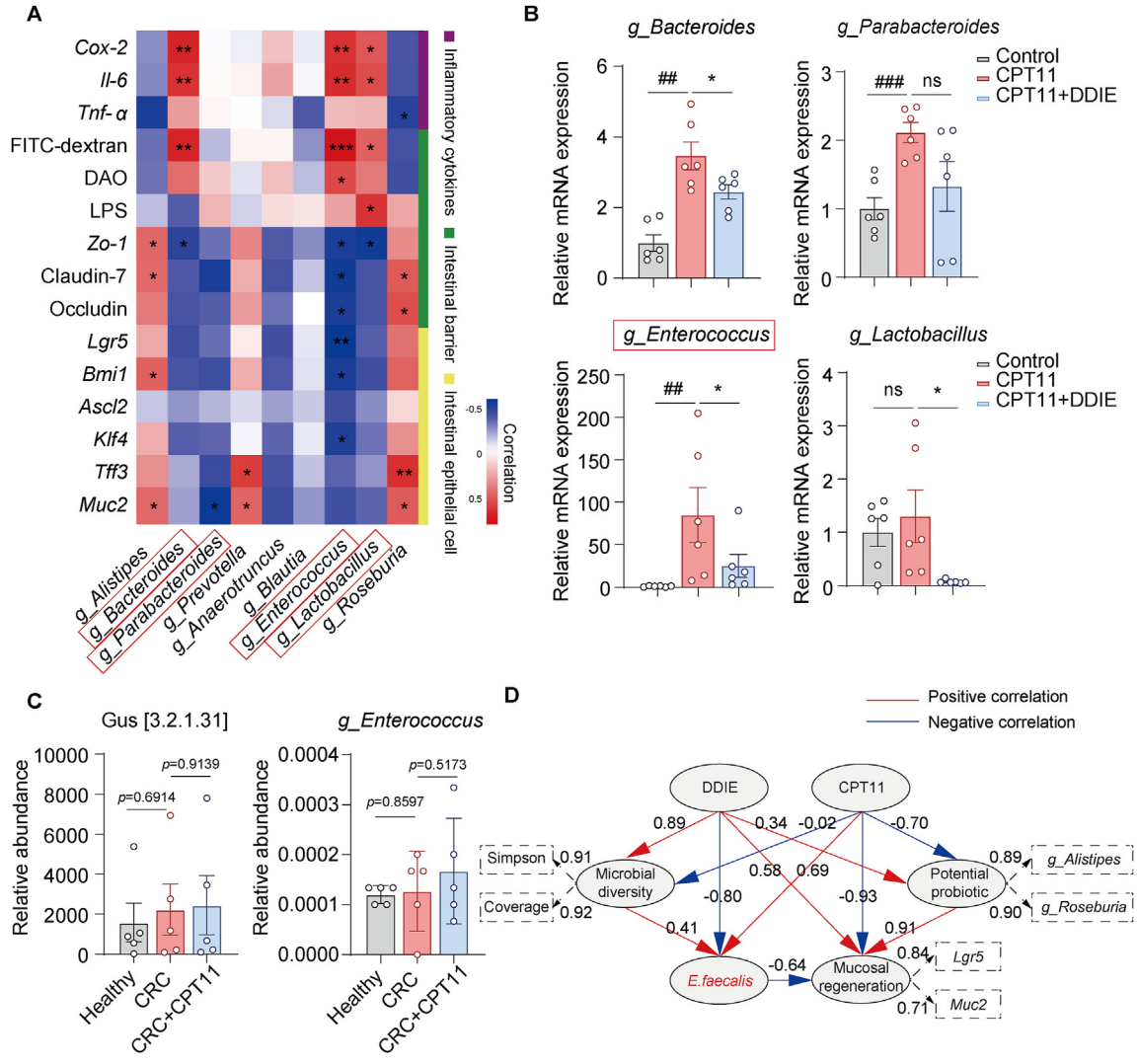

Figure 6 The Gus-generating bacterial strain *E. faecalis* exhibited negative correlations with ISCs differentiation markers, DDIE reversed the elevated abundance of *E. faecalis* in CPT11-induced mucositis mice. (A) Heatmap of Spearman's correlation analysis between the Gus-producing bacteria and inflammatory cytokines, intestinal barrier, and intestinal epithelial cell-related index in mice. Red color represents a positive correlation, while blue represents a negative correlation ($n = 6$). (B) mRNA levels of *g_Bacteroides*, *g_Parabacteroides*, *g_Enterococcus*, and *g_Lactobacillus* in feces ($n = 6$). (C) Proportional abundance of ortholog K01195 (KO: K01195; description: beta-glucuronidase [EC: 3.2.1.31]) and the relative abundance of *g_Enterococcus* in healthy subjects, colorectal cancer patients receiving (CRC+CPT11) or not receiving CPT11 chemotherapy (CRC) ($n = 5$). (D) Partial Least Squares Path Modeling (PLS-PM) showed the complex redundant relationships of different variable factors. An observable variable or a latent variable is presented by a box. Dashed rectangles display the loadings for microbial diversity, potential probiotics, and mucosal regeneration as latent variables. Path coefficients, derived from 1000 bootstraps, are shown as lines where red line indicates a positive relationship and blue line a negative one. A dashed arrow represents a coefficient not significantly different from 0 ($P > 0.05$). The GoF statistic is used to evaluate the model, and the GoF value is 0.74. Data are expressed as mean ± SEM. $^{\#\#}P < 0.01$, $^{\#\#\#}P < 0.001$ *vs.* Control group; $^{*}P < 0.05$ *vs.* CPT11 group. ns, not significant.

or SN38 on the organoids, leading to an improvement in MUC2 expression. Additionally, *E. faecalis* was co-incubated with DDIE at different concentrations (0, 50, 100, and 200 μmol/L), as illustrated in Fig. 7J. Notably, at 6 h, DDIE exhibited its most potent inhibitory effect on *E. faecalis*.

Since SN38 is enzymatically converted from SN38G by Gus-expressing bacteria, which directly induces mucositis, we further incubated organoids with a combination of *E. faecalis* and SN38G. Co-incubation of organoids with a combination of *E. faecalis* and SN38G resulted in a noticeable reduction in organoid-forming efficiency, organoid surface area, and the expression of KI67 and MUC2 compared to organoids treated with SN38G alone (Fig. 7I). To further support the promotive effect of DDIE on the proliferation and differentiation of ISCs, we incubated organoids with a combination of *E. faecalis* and SN38G in the presence or absence of DDIE (15 μmol/L). Administration of DDIE potentially and partially mitigated the effect of *E. faecalis* on the conversion of SN38G to SN38, thereby leading to an improvement in the organoid-forming efficiency, organoid surface area, and the expression of KI67 and MUC2 (Fig. 7I).

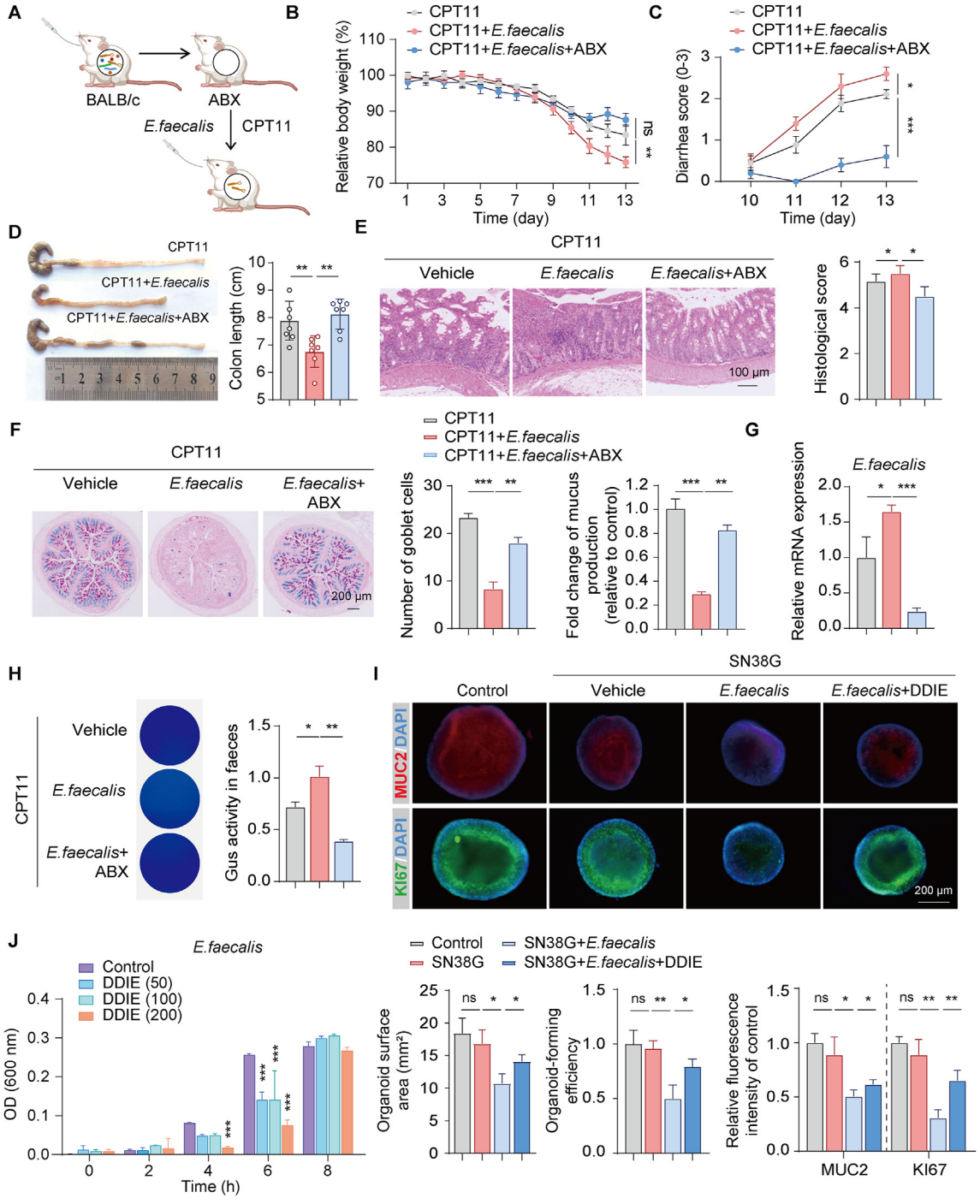

Figure 7 Colonization of *E. faecalis* exacerbated CPT11-induced gut mucositis. (A) Schematic diagram of the experimental procedure. (B) Body weight was recorded following the animal experiment. Data were plotted as a percentage of basal body weight. Data are expressed as mean ± SEM ($n = 6$). (C) Diarrhea scores were evaluated as described in Methods. Data are expressed as mean ± SEM ($n = 6$). (D) The colon was photographed and colon length was measured ($n = 6$). (E) H&E staining and histopathological scores of colon sections ($n = 6$). (F) Representative AB-PAS staining of colonic sections, the counting of goblet cells per villus calculation unit, and the assessment of mucus production ($n = 3$). (G) mRNA levels of *E. faecalis* in feces ($n = 6$). (H) Gus-producing bacteria in feces were detected by agar medium supplemented with 4-MUG, and the Gus activity was assessed by PNPG assay ($n = 6$). (I) Representative immunofluorescence images (MUC2: red; KI67: green; DAPI: blue) of colonic organoids are shown (upper panel). Qualitative statistics of the organoid-forming efficiency, organoid surface area, and MUC2 and KI67 fluorescence intensity of the organoids (lower panel). (J) Effects of DDIE (0, 50, 100, 200 μmol/L) on the propagation of *E. faecalis* by *in vitro* co-incubation experiment ($n = 3$). Data are expressed as mean ± SD. $^*P < 0.05$, $^{**}P < 0.01$, and $^{***}P < 0.001$. ns, not significant.

Collectively, these data suggest that *E. faecalis* plays a contributory role in the disruption of epithelial regeneration induced by CPT11, indicating that the enhancement of epithelial repair by DDIE in CPT11-induced mucositis mice may be attributed to the inhibition of *E. faecalis*.

3.7. DDIE exhibited a synergistic antitumor effect with CPT11 in colorectal tumor-bearing mice

Considering the decrease in the intestinal lumen of SN38 level in mice receiving DDIE administration, concerns arose about the potential impact of DDIE on the anticancer efficacy of CPT11. In an experimental BALB/c mouse model with transplanted murine colorectal cancer cells (CT26), treatment with CPT11 significantly reduced tumor size, weight, and volume (Supporting Information Fig. S6A−S6D). Notably, the combination of DDIE and CPT11 resulted in a significant slowdown of tumor growth compared to CPT11 treatment alone. Subsequently, the CCK-8 experiment demonstrated a dose-dependent inhibitory effect of DDIE or SN38 on CT26 cells (Fig. S6E and S6F). The combined index (CI) was employed to assess the synergistic efficacy of the drugs, uncovering a synergistic inhibitory effect of DDIE and SN38 on CT26 cells (Fig. S6G).

These data suggest that DDIE effectively mitigates CPT11-induced mucositis without compromising the antitumor effect of CPT11.

4. Discussion

CPT11-induced gut mucositis manifested as intestinal epithelial injury, diarrhea, and inflammation of the bowel wall. The initial indication of this adverse reaction was observed as a decline in body weight in CPT11-treated mice[12]. However, in the present study, upon administering DDIE at doses of 25 or 75 mg/kg, the rate of weight loss in mice was mitigated. Notably, mice exhibited a more accelerated weight loss after discontinuing CPT11 treatment, resembling the characteristics of late-onset diarrhea. This harmful effect was accompanied by a substantial reduction in colon length. Additionally, CPT11-treated mice experienced significant damage to colonic tissue, marked by detached villi and impaired crypts, while DDIE administration alleviated this damage, demonstrating promising therapeutic effects against CPT11-induced mucositis.

Prior studies have established a connection between gut mucositis and heightened levels of inflammatory cytokines[35]. The increase in inflammation is particularly associated with TNF-α and IL-6, known for their roles in activating neutrophils and lymphocytes, thereby initiating the body's immune response[36]. Furthermore, iNOS and COX-2, acting as downstream inflammatory mediators in the NF-κB signaling pathway, are responsible for the synthesis of the inflammatory factors nitric oxide (NO) and prostaglandin E2 (PGE2), respectively[37]. In alignment with earlier research, our results suggest that DDIE significantly mitigated the CPT11-induced upregulation of TNF-α, IL-6, iNOS, and COX-2 in colon tissues.

The well-established association between CPT11 chemotherapy and intestinal toxicity is primarily attributed to damage to the intestinal barrier[38]. This barrier consists of intestinal epithelial cells, the tight junctions between these cells, and the mucous layers that envelop them[39]. ZO-1 is a cytoplasmic protein that collaborates with transmembrane proteins such as Occludin and Claudin. This interaction establishes robust connections between adjacent intestinal epithelial cells, forming an effective shield that safeguards the intestinal epithelium against the invasion of toxic macromolecules and pathogenic microorganisms[39]. In the present study, we observed a significant restoration of tight junction proteins (ZO-1 and Occludin) in the intestinal mucosa after DDIE treatment, effectively countering the decrease induced by CPT11. Additionally, the degree of intestinal mucosal injury is reported to be positively correlated with FITC-dextran, LPS, and DAO[40]. Correspondingly, our study demonstrated a remarkable decrease in FITC-dextran, LPS, and DAO levels in DDIE-treated mice. Furthermore, transmission electron microscopy revealed a well-preserved and tightly connected intestinal epithelial barrier in DDIE-treated mice.

To gain a deeper understanding of the mechanisms underlying the recovery effect of DDIE, we conducted transcriptomic analysis on colonic tissue. The results highlighted a significant enrichment in gene pathways related to the inflammatory response and intestinal epithelium development. Subsequent gene heatmap analysis and RT-qPCR validation demonstrated that DDIE effectively restored the downregulated expression of ISC and goblet cell marker genes induced by CPT11. The crucial role of ISCs in regenerating the intestinal epithelium, through self-renewal and differentiation into various intestinal epithelial cell types, has been well-established. Goblet cells, known for secreting mucin and forming the protective mucus barrier, are key components in this process[39]. Our subsequent study revealed a notable increase in colonic goblet cell number and mucin-like glycoprotein following DDIE administration. Furthermore, transmission electron microscopy exposed an amplified accumulation of mucin granules within colonic goblet cells in DDIE-treated mice. These findings underscore the potential of DDIE to enhance the self-renewal and differentiation of ISCs into goblet cells, a crucial process for mucin production and maintaining intestinal mucosal integrity during CPT11-induced mucositis.

The intestinal metabolism of CPT11 and its metabolites, SN38 and SN38G, plays a crucial role in the onset of diarrhea and is intricately linked with the activity of the bacterial Gus enzyme[41]. Under the action of the Gus enzyme, SN38G can be converted back into an enterotoxic metabolite, SN38, leading to intestinal epithelial cell necrosis and compromised intestinal mucosal barrier function[42]. As early as 1995, it was proposed that intestinal Gus might be responsible for the dose-limiting adverse reactions of the anticancer drug CPT11[43]. In 2010, a pivotal study validated the involvement of intestinal Gus in the toxicity of CPT11 and unveiled the potential of microbial Gus-specific inhibitors to ameliorate intestinal injury and diarrhea[44]. Notably, an estimated 45% of gut bacteria in the human microbiome database encode Gus, including *Bacteroides*, *Alistipes*, *Parabacteroides*, *Prevotella*, *Anaerotruncus*, *Blautia*, and *Enterococcus*[45]. In this context, we examined the abundance of Gus-expressing bacteria through 16S rRNA sequencing. As anticipated, the data validated our hypothesis, revealing that DDIE remarkably diminished the population of GUS-generating bacteria and the Gus enzyme induced by CPT11 in the feces. These findings were corroborated by *in vitro* assays, which demonstrated the inhibitory effect of DDIE on the Gus enzyme and fecal SN38 levels, and by molecular docking studies that further supported the Gus-inhibitory effect of DDIE.

Accumulating evidence increasingly emphasizes the crucial role of gut microbiota in sustaining a healthy intestinal epithelial barrier, GI motor function, metabolism, and the immune system[46,47]. Gut dysbiosis often manifests as reduced diversity in gut microbiota, a characteristic feature in patients with inflammatory bowel disease and chemotherapy-related intestinal mucositis[47]. To assess the fecal

microbiota composition in mice, we conducted 16S rRNA sequencing. As expected, treatment with CPT11 led to a significant decrease in fecal microbiota diversity. However, upon the administration of DDIE, the diversity of the microbiota was notably restored, and its composition showed higher similarity to that of the control mice. Detailed analysis of the abundance of various bacterial genera showed that CPT11 treatment increased the abundance of *g_Enterococcus*, which was markedly decreased by DDIE administration. To confirm the involvement of the gut microbiota in alleviating CPT11-induced mucositis by DDIE, we established a pseudo-germ-free mouse model and conducted FMT experiments. We found that the fecal microbiota transplanted from DDIE-treated mice effectively mitigated CPT11-induced mucositis. Nevertheless, when the gut microbiota was depleted using an antibiotic cocktail, the previously observed effects of DDIE on CPT11-induced intestinal injury became imperceptible, significantly reinforcing the essential role of the gut microbiota. Additionally, the abundance of colonic *g_Enterococcus* was increased in CPT11-FMT mice, which was significantly reduced in CPT11+DDIE-FMT mice. RT-qPCR analysis confirmed the increased abundance of *g_Enterococcus* in the feces of the CPT11 group, while DDIE effectively attenuated this trend. The subsequent correlation analysis suggested that *g_Enterococcus* exhibits positive correlations with *Cox-2*, *Il-6*, and FITC-dextran, while showing negative correlations with *Zo-1*, Claudin-7, and Occludin. These findings underscore the specific influence of DDIE in modulating the gut microbiota composition, particularly in reducing the abundance of *g_Enterococcus*, which may contribute to the attenuating effects of DDIE against CPT11-induced mucositis.

To link our findings with clinical research, we conducted an analysis of the abundance of the genus *g_Enterococcus* in fecal 16S rRNA sequencing data obtained from European Nucleotide Archive. The dataset comprised samples from healthy individuals and patients with colorectal cancer, further categorized into those undergoing CPT11 chemotherapy (CRC + CPT11) and those not undergoing CPT11 chemotherapy (CRC). Our findings indicated an increased presence of *g_Enterococcus* in the fecal samples of colorectal cancer patients undergoing CPT11 chemotherapy compared to both healthy subjects and colorectal cancer patients not receiving CPT11 chemotherapy; however, this increase did not reach statistical significance. In subsequent FMT experiments, we observed the presence of the *Enterococcus* genus and its two species, *E. faecalis* and *E. faecium*, in the feces of CPT11-FMT mice. Intriguingly, the fecal microbiota transplanted from DDIE-treated mice exhibited the capability to effectively reduce the abundance of *E. faecalis*, while demonstrating no significant impact on *E. faecium*.

E. faecalis has been reported to exacerbate experimental colitis through mediating glucosamine metabolism[48]. Other studies have demonstrated that *E. faecalis* encodes the Gus enzyme[49], suggesting its potential involvement in intestinal mucosal injury. By constructing a PLS-PM algorithm model, we are able to reveal a complex interplay among bacterial diversity, potential probiotics, the Gus-producing bacterium *E. faecalis*, and intestinal mucosal regeneration. The model suggests that *E. faecalis* plays a critical role in the disruption of the intestinal mucosal barrier caused by CPT11, and DDIE primarily functions by inhibiting *E. faecalis*, thus facilitating mucosal regeneration. To delve into the putative role of how *E. faecalis* acts, we conducted experiments by colonizing *E. faecalis* in the intestines of pseudo-germ-free mice with mucositis. As anticipated, the data from *E. faecalis* colonization experiments revealed a significant exacerbation of intestinal mucositis, accompanied by an apparent increase in intestinal Gus-generating bacteria and the levels of Gus and SN38. Collectively, our study demonstrated that DDIE effectively alleviated CPT11-induced intestinal mucosal injury by inhibiting Gus-expressing *E. faecalis*. This resulted in reduced levels of Gus and SN38 in the intestinal lumen, indirectly promoting the proliferation and differentiation of ISCs to repair mucosal damage caused by CPT11.

Nevertheless, the reduction of intestinal lumen SN38 level by DDIE raises concerns regarding its potential impact on the anti-colorectal cancer efficacy of CPT11. Indeed, DDIE is reported to suppress colorectal cancer by enhancing cellular autophagy through the promotion of endoplasmic reticulum stress[48]. In our study, DDIE exhibited certain synergistic inhibitory effects on colorectal cancer when combined with CPT11 in subcutaneous colorectal cancer xenograft mouse model. However, the precise mechanisms underlying this inhibitory effect require further experimental validation. Additionally, *in vitro* assays confirmed the anti-tumor activity of DDIE against HCT116 and CT26 colorectal cancer cells, providing further support for the anti-colorectal cancer effects of DDIE in mice. Notably, *E. faecalis* has been implicated in promoting a migratory and invasive phenotype in colon cancer cells[46]. Therefore, the inhibition of *E. faecalis* by DDIE may also contribute to the synergistic anti-tumor effect with CPT11.

5. Conclusions

The intestinal epithelium maintains homeostasis through the continuous self-renewal and differentiation of ISCs. Our research elucidates how this natural restorative mechanism becomes compromised by the potent cytotoxic effects of SN38, the active metabolite of CPT11, which impairs the intestinal epithelial self-renewal process. Through a comprehensive array of experimental methodologies, we have demonstrated that DDIE effectively counteracts this detrimental effect by targeting Gus-expressing *E. faecalis*. By inhibiting the proliferation of these bacteria, DDIE indirectly prevents the conversion of SN38G to toxic SN38. Consequently, this inhibition of bacterial activity may promote the proliferation and differentiation of ISCs, thus facilitating the repair of intestinal mucosal damage caused by CPT11 exposure. Our study provides insights into the molecular and microbial mechanisms involved in CPT11-induced gut mucositis and underscores the potential therapeutic application of DDIE in mitigating CPT11 chemotoxicity through its impact on the Gus-expressing bacterium *E. faecalis*. These findings offer novel perspectives on targeting Gus-generating bacteria to counteract chemotherapy-induced GI toxicity by enhancing the regeneration and repair of ISCs. Moreover, DDIE demonstrated synergistic anti-cancer effects while mitigating the intestinal toxicity induced by CPT11, suggesting the potential of DDIE or its derivative as an adjuvant treatment for CPT11 chemotherapeutic therapy in clinic. Limitations of the study include reliance on animal models, a limited understanding of DDIE's long-term effects and mechanisms on gut microbiota modulation, and the absence of clinical trial data for human validation. Future research endeavors may involve: (i) further identifying Gus-generating bacterial species implicated in the toxicity of CPT11 chemotherapy; (ii) facilitating the development of Gus-generating bacteria suppressors; (iii) pursuing strategies to promote epithelial regeneration for the prevention of chemotherapy-associated GI adverse reactions. Additionally, employing computational simulations to refine and

tailor the chemical structure of DDIE, optimizing its pharmacological properties for enhanced therapeutic efficacy. Furthermore, rigorous clinical trial analyses and verification are imperative to substantiate the potential of DDIE as an adjuvant therapy in clinical settings, particularly in augmenting the outcomes of chemotherapy and ameliorating CPT11-induced mucositis.

Availability and implementation

Microbiological data available at NCBI *via* BioProject ID PRJNA797942.

Acknowledgments

The author would like to thank Marwa S Mahdy et al. (Beni-Suef University) for providing clinical data (approval number: FMBSUREC/05072020/Mahdy). We would like to express our great appreciation to Prof. Ling Zhao (Shanghai University of Traditional Chinese Medicine) for valuable and constructive suggestions during the research. This research was supported by the National Natural Science Foundation of China (No. 82274329, 82304991, 82130115), the China Postdoctoral Science Foundation (No. 2023M732336), and the Shanghai Science and Technology Committee Sailing Program Foundation (No. 23YF1442500, China).

Author contributions

Ruiyang Gao and Bei Yue conceptualized the project and carried out the experiments; Cheng Lv, Xiaolong Geng, Zhilun Yu, and Hao Wang participated in part of the experiment; Beibei Zhang, Fangbin Ai, Ziyi Wang and Donghui Liu contributed to data collection and analysis; Rruiyang Gao and Bei Yue participated in the drafting of the article; Wei Dou, Ruiyang Gao and Bei Yue designed the study and wrote the manuscript; Wei Dou, Zhengtao Wang and Bei Yue provided grant support; Kaixian Chen, Zhengtao Wang and Wei Dou supervised the study. All authors read and approved the submitted manuscript.

Conflicts of interest

The authors declare no conflicts of interest.

Appendix A. Supporting information

Supporting information to this article can be found online at https://doi.org/10.1016/j.apsb.2024.09.018.

References

1. Bailly C. Irinotecan: 25 years of cancer treatment. *Pharmacol Res* 2019;**148**:104398.
2. Wang Y, Wei B, Wang D, Wu J, Gao J, Zhong H, et al. DNA damage repair promotion in colonic epithelial cells by andrographolide downregulated cGAS−STING pathway activation and contributed to the relief of CPT-11-induced intestinal mucositis. *Acta Pharm Sin B* 2022;**12**:262−73.
3. Kciuk M, Marciniak B, Kontek R. Irinotecan-still an important player in cancer chemotherapy: a comprehensive overview. *Int J Mol Sci* 2020;**21**:4919.
4. Yue B, Gao R, Wang Z, Dou W. Microbiota−host−irinotecan axis: a new insight toward irinotecan chemotherapy. *Front Cel Infect Microbiol* 2021;**11**:710945.
5. He S, Lei P, Kang W, Cheung P, Xu T, Mana M, et al. Stiffness restricts the stemness of the intestinal stem cells and skews their differentiation toward goblet cells. *Gastroenterology* 2023;**164**:1137−51.
6. He Y, Ma J, Fan X, Ding L, Ding X, Zhang QY, et al. The key role of gut−liver axis in pyrrolizidine alkaloid-induced hepatotoxicity and enterotoxicity. *Acta Pharm Sin B* 2021;**11**:3820−35.
7. Thorpe D, Butler R, Sultani M, Vanhoecke B, Stringer A. Irinotecan-induced mucositis is associated with goblet cell dysregulation and neural cell damage in a tumour bearing DA rat model. *Pathol Oncol Res* 2020;**26**:955−65.
8. Lam W, Jiang Z, Guan F, Hu R, Liu SH, Chu E, et al. The number of intestinal bacteria is not critical for the enhancement of antitumor activity and reduction of intestinal toxicity of irinotecan by the Chinese herbal medicine PHY906 (KD018). *BMC Complement Altern Med* 2014;**14**:490.
9. Chamseddine AN, Ducreux M, Armand JP, Paoletti X, Satar T, Paci A, et al. Intestinal bacterial β-glucuronidase as a possible predictive biomarker of irinotecan-induced diarrhea severity. *Pharmacol Ther* 2019;**199**:1−15.
10. Gan C, Wang J, Martinez-Chavez A, Hillebrand M, de Vries N, Beukers J, et al. Carboxylesterase 1 family knockout alters drug disposition and lipid metabolism. *Acta Pharm Sin B* 2023;**13**:618−31.
11. Lin HY, Chen CY, Lin TC, Yeh LF, Hsieh WC, Gao S, et al. Entropy-driven binding of gut bacterial β-glucuronidase inhibitors ameliorates irinotecan-induced toxicity. *Commun Biol* 2021;**4**:280.
12. Cheng KW, Tseng CH, Tzeng CC, Leu YL, Cheng TC, Wang JY, et al. Pharmacological inhibition of bacterial β-glucuronidase prevents irinotecan-induced diarrhea without impairing its antitumor efficacy *in vivo*. *Pharmacol Res* 2019;**139**:41−9.
13. Kong R, Liu T, Zhu X, Ahmad S, Williams AL, Phan AT, et al. Old drug new use-amoxapine and its metabolites as potent bacterial β-glucuronidase inhibitors for alleviating cancer drug toxicity. *Clin Cancer Res* 2014;**20**:3521−30.
14. Takasuna K, Kasai Y, Kitano Y, Mori K, Kobayashi R, Hagiwara T, et al. Protective effects of kampo medicines and baicalin against intestinal toxicity of a new anticancer camptothecin derivative, irinotecan hydrochloride (CPT-11), in rats. *Jpn J Cancer Res* 1995;**86**:978−84.
15. Lam W, Bussom S, Guan F, Jiang Z, Zhang W, Gullen EA, et al. The four-herb Chinese medicine PHY906 reduces chemotherapy-induced gastrointestinal toxicity. *Sci Transl Med* 2010;**2**:45r−59r.
16. Wang C, Teng X, Wang C, Liu B, Zhou R, Xu X, et al. Insight into the mechanism of Xiao-Chai-Hu-Tang alleviates irinotecan-induced diarrhea based on regulating the gut microbiota and inhibiting gut β-GUS. *Phytomedicine* 2023;**120**:155040.
17. Lietzan AD, Simpson JB, Walton WG, Jariwala PB, Xu Y, Boynton MH, et al. Microbial β-glucuronidases drive human periodontal disease etiology. *Sci Adv* 2023;**9**:g3390.
18. Jariwala PB, Pellock SJ, Goldfarb D, Cloer EW, Artola M, Simpson JB, et al. Discovering the microbial enzymes driving drug toxicity with activity-based protein profiling. *ACS Chem Biol* 2020;**15**:217−25.
19. Mroczynska M, Libudzisz Z. β-Glucuronidase and β-glucosidase activity of Lactobacillus and Enterococcus isolated from human feces. *Pol J Microbiol* 2010;**59**:265−9.
20. Fernandes MR, Aggarwal P, Costa R, Cole AM, Trinchieri G. Targeting the gut microbiota for cancer therapy. *Nat Rev Cancer* 2022;**22**:703−22.
21. Ashokkumar K, Simal-Gandara J, Murugan M, Dhanya MK, Pandian A. Nutmeg (myristica fragrans houtt.) Essential oil: a review on its composition, biological, and pharmacological activities. *Phytother Res* 2022;**36**:2839−51.
22. Li F, Yang XW. Determination of dehydrodiisoeugenol in rat tissues using HPLC method. *Biomed Chromatogr* 2008;**22**:1206−12.

23. Godinez-Chaparro B, Perez-Gutierrez S, Perez-Ramos J, Heyerdahl-Viau I, Hernandez-Vazquez L. Synthesis and biological activities of dehydrodiisoeugenol: a review. *Pharmaceuticals* 2022;**15**:1351.
24. Xu J, Li X, Yuan Z, Li F, Xu Z. Mitigative effects of dehydrodiisoeugenol on enteritis and co-occurring dysmotility in murine model. *Pak J Pharm Sci* 2022;**35**:1347−55.
25. Yue B, Gao R, Lv C, Yu Z, Wang H, Geng X, et al. Berberine improves irinotecan-induced intestinal mucositis without impairing the anti-colorectal cancer efficacy of irinotecan by inhibiting bacterial β-glucuronidase. *Front Pharmacol* 2021;**12**:774560.
26. Dong S, Zhu M, Wang K, Zhao X, Hu L, Jing W, et al. Dihydromyricetin improves DSS-induced colitis in mice *via* modulation of fecal-bacteria-related bile acid metabolism. *Pharmacol Res* 2021;**171**:105767.
27. Qu Y, Li X, Xu F, Zhao S, Wu X, Wang Y, et al. Kaempferol alleviates murine experimental colitis by restoring gut microbiota and inhibiting the LPS−TLR4−NF-κB axis. *Front Immunol* 2021;**12**:679897.
28. Qi X, Zhang Y, Zhang Y, Luo F, Song K, Wang G, et al. Vitamin b_{12} produced by cetobacterium somerae improves host resistance against pathogen infection through strengthening the interactions within gut microbiota. *Microbiome* 2023;**11**:135.
29. Mahdy MS, Azmy AF, Dishisha T, Mohamed WR, Ahmed KA, Hassan A, et al. Irinotecan−gut microbiota interactions and the capability of probiotics to mitigate irinotecan-associated toxicity. *BMC Microbiol* 2023;**23**:53.
30. Yu Z, Yue B, Ding L, Luo X, Ren Y, Zhang J, et al. Activation of PXR by alpinetin contributes to abrogate chemically induced inflammatory bowel disease. *Front Pharmacol* 2020;**11**:474.
31. Zheng D, Liao H, Chen S, Liu X, Mao C, Zhang C, et al. Elevated levels of circulating biomarkers related to leaky gut syndrome and bacterial translocation are associated with graves' disease. *Front Endocrinol* 2021;**12**:796212.
32. Gustafsson JK, Johansson M. The role of goblet cells and mucus in intestinal homeostasis. *Nat Rev Gastroenterol Hepatol* 2022;**19**:785−803.
33. Yue B, Yu ZL, Lv C, Geng XL, Wang ZT, Dou W. Regulation of the intestinal microbiota: an emerging therapeutic strategy for inflammatory bowel disease. *World J Gastroenterol* 2020;**26**:4378−93.
34. Lindop R, Tasman-Jones C, Thomsen LL, Lee SP. Cellulose and pectin alter intestinal β-glucuronidase (ec 3.2.1.31) in the rat. *Br J Nutr* 1985;**54**:21−6.
35. Chen Y, Cui W, Li X, Yang H. Interaction between commensal bacteria, immune response and the intestinal barrier in inflammatory bowel disease. *Front Immunol* 2021;**12**:761981.
36. Wen Y, Rudemiller NP, Zhang J, Robinette T, Lu X, Ren J, et al. TNF-α in T lymphocytes attenuates renal injury and fibrosis during nephrotoxic nephritis. *Am J Physiol Ren Physiol* 2020;**318**:F107−16.
37. Ren Q, Guo F, Tao S, Huang R, Ma L, Fu P. Flavonoid fisetin alleviates kidney inflammation and apoptosis *via* inhibiting Src-mediated NF-κB p65 and MAPK signaling pathways in septic AKI mice. *Biomed Pharmacother* 2020;**122**:109772.
38. Quintanilha MF, Miranda VC, Souza RO, Gallotti B, Cruz C, Santos EA, et al. *Bifidobacterium longum* subsp. Longum 5^{1A} attenuates intestinal injury against irinotecan-induced mucositis in mice. *Life Sci* 2022;**289**:120243.
39. Rose EC, Odle J, Blikslager AT, Ziegler AL. Probiotics, prebiotics and epithelial tight junctions: a promising approach to modulate intestinal barrier function. *Int J Mol Sci* 2021;**22**:6729.
40. Zhuang S, Zhong J, Bian Y, Fan Y, Chen Q, Liu P, et al. Rhein ameliorates lipopolysaccharide-induced intestinal barrier injury *via* modulation of Nrf2 and MAPKs. *Life Sci* 2019;**216**:168−75.
41. Sharkey RM, Mcbride WJ, Cardillo TM, Govindan SV, Wang Y, Rossi EA, et al. Enhanced delivery of SN-38 to human tumor xenografts with an anti-Trop-2−SN-38 antibody conjugate (sacituzumab govitecan). *Clin Cancer Res* 2015;**21**:5131−8.
42. Sun R, Zhu L, Li L, Song W, Gong X, Qi X, et al. Irinotecan-mediated diarrhea is mainly correlated with intestinal exposure to SN-38: critical role of gut Ugt. *Toxicol Appl Pharmacol* 2020;**398**:115032.
43. Kudoh S, Fukuoka M, Masuda N, Yoshikawa A, Kusunoki Y, Matsui K, et al. Relationship between the pharmacokinetics of irinotecan and diarrhea during combination chemotherapy with cisplatin. *Jpn J Cancer Res* 1995;**86**:406−13.
44. Wallace BD, Wang H, Lane KT, Scott JE, Orans J, Koo JS, et al. Alleviating cancer drug toxicity by inhibiting a bacterial enzyme. *Science* 2010;**330**:831−5.
45. Pollet RM, D'Agostino EH, Walton WG, Xu Y, Little MS, Biernat KA, et al. An atlas of β-glucuronidases in the human intestinal microbiome. *Structure* 2017;**25**:967−77.
46. Adak A, Khan MR. An insight into gut microbiota and its functionalities. *Cell Mol Life Sci* 2019;**76**:473−93.
47. Chen Y, Zhou J, Wang L. Role and mechanism of gut microbiota in human disease. *Front Cel Infect Microbiol* 2021;**11**:625913.
48. Williamson AJ, Jacobson R, van Praagh JB, Gaines S, Koo HY, Lee B, et al. *Enterococcus faecalis* promotes a migratory and invasive phenotype in colon cancer cells. *Neoplasia* 2022;**27**:100787.
49. Yang W, Wei B, Yan R. Amoxapine demonstrates incomplete inhibition of β-glucuronidase activity from human gut microbiota. *SLAS Discov* 2018;**23**:76−83.